Discovery of ASKAP J173608.2–321635 as a Highly Polarized Transient Point Source with the Australian SKA Pathfinder

Ziteng Wang[1,2,3], David L. Kaplan[4], Tara Murphy[1,3], Emil Lenc[2], Shi Dai[5], Ewan Barr[6], Dougal Dobie[3,7], B. M. Gaensler[8,9], George Heald[10], James K. Leung[1,2,3], Andrew O'Brien[4], Sergio Pintaldi[11], Joshua Pritchard[1,2,3], Nanda Rea[12,13], Gregory R. Sivakoff[14], B. W. Stappers[15], Adam Stewart[1], E. Tremou[16], Yuanming Wang[1,2,3], Patrick A. Woudt[17], and Andrew Zic[2,18]

[1] Sydney Institute for Astronomy, School of Physics, University of Sydney, Sydney, New South Wales 2006, Australia; zwan4817@uni.sydney.edu.au, tara.murphy@sydney.edu.au
[2] ATNF, CSIRO Space and Astronomy, PO Box 76, Epping, New South Wales 1710, Australia
[3] ARC Centre of Excellence for Gravitational Wave Discovery (OzGrav), Hawthorn, Victoria, Australia
[4] Center for Gravitation, Cosmology, and Astrophysics, Department of Physics, University of Wisconsin-Milwaukee, P.O. Box 413, Milwaukee, WI 53201, USA
[5] School of Science, Western Sydney University, Locked Bag 1797, Penrith South DC, NSW 2751, Australia
[6] Max-Planck-Institut für Radioastronomie, Auf dem Hügel 69, D-53121 Bonn, Germany
[7] Centre for Astrophysics and Supercomputing, Swinburne University of Technology, Hawthorn, Victoria, Australia
[8] Dunlap Institute for Astronomy and Astrophysics, University of Toronto, 50 St. George St., Toronto, ON M5S 3H4, Canada
[9] David A. Dunlap Department of Astronomy and Astrophysics, University of Toronto, 50 St. George St., Toronto, ON M5S 3H4, Canada
[10] CSIRO Space and Astronomy, PO Box 1130, Bentley WA 6102, Australia
[11] Sydney Informatics Hub, The University of Sydney, NSW 2008, Australia
[12] Institute of Space Sciences (ICE, CSIC), Campus UAB, Carrer de Can Magrans s/n, E-08193, Barcelona, Spain
[13] Institut d'Estudis Espacials de Catalunya (IEEC), Carrer Gran Capità 2-4, E-08034 Barcelona, Spain
[14] Department of Physics, University of Alberta, CCIS 4-181, Edmonton, AB T6G 2E1, Canada
[15] Jodrell Bank Centre for Astrophysics, Department of Physics and Astronomy, The University of Manchester, Manchester M13 9PL, UK
[16] LESIA, Observatoire de Paris, CNRS, PSL Research University, Sorbonne Université, Université de Paris, Meudon, France
[17] Inter-University Institute for Data-Intensive Astronomy, Department of Astronomy, University of Cape Town, Private Bag X3, Rondebosch 7701, South Africa
[18] Department of Physics and Astronomy, and Research Centre in Astronomy, Astrophysics and Astrophotonics, Macquarie University, NSW 2109, Australia

Abstract

We report the discovery of a highly polarized, highly variable, steep-spectrum radio source, ASKAP J173608.2 −321635, located ∼4° from the Galactic Center in the Galactic plane. The source was detected six times between 2020 January and 2020 September as part of the Australian Square Kilometre Array Pathfinder Variables and Slow Transients (ASKAP VAST) survey at 888 MHz. It exhibited a high degree (∼25%) of circular polarization when it was visible. We monitored the source with the MeerKAT telescope from 2020 November to 2021 February on a 2–4 week cadence. The source was not detected with MeerKAT before 2021 February 7 when it appeared and reached a peak flux density of 5.6 mJy. The source was still highly circularly polarized, but also showed up to 80% linear polarization, and then faded rapidly with a timescale of one day. The rotation measure of the source varied significantly, from -11.8 ± 0.8 rad m^{-2} to -64.0 ± 1.5 rad m^{-2} over three days. No X-ray counterpart was found in follow-up Swift or Chandra observations about a week after the first MeerKAT detection, with upper limits of $\sim 5.0 \times 10^{31}$ erg s^{-1} (0.3–8 keV, assuming a distance ∼10 kpc). No counterpart is seen in new or archival near-infrared observations down to $J = 20.8$ mag. We discuss possible identifications for ASKAP J173608.2−321635 including a low-mass star/substellar object with extremely low infrared luminosity, a pulsar with scatter-broadened pulses, a transient magnetar, or a Galactic Center radio transient: none of these fully explains the observations, which suggests that ASKAP J173608.2−321635 may represent part of a new class of objects being discovered through radio imaging surveys.

Unified Astronomy Thesaurus concepts: Radio transient sources (2008); Galactic radio sources (571); Neutron stars (1108); Magnetars (992); Galactic center (565)

1. Introduction

Many types of Galactic sources are known to be variable at radio wavelengths, including pulsars, stars, and magnetars. For example, Staelin & Reifenstein (1968) detected giant radio pulses from the Crab pulsar, Hallinan et al. (2007) found periodic radio bursts from the M9 dwarf TVLM 513–46546, and Camilo et al. (2006) detected transient pulsed radio emission from the magnetar XTE J1810–197. Exploring the radio variability can help us better understand extreme astrophysical phenomena and probably find unexpected sources (Fender et al. 2015).

The development of large field-of-view radio interferometers, such as the Australian Square Kilometre Array Pathfinder (ASKAP; Hotan et al. 2021), enables us to investigate variable and transient phenomena more systematically over a wider parameter space. The ASKAP survey for Variables and Slow Transients[19] (VAST; Murphy et al. 2013), is designed to search for such sources. The VAST Phase I Pilot Survey (VAST-P1; Murphy et al. 2021) was conducted between 2019 August and 2020 August. The footprint of VAST-P1 consists of six regions including a ∼250 deg^2 region covering the Galactic Center (with $\sim 356° < l < 10°$, $|b| < \sim 5°$). We used the VAST Transient detection pipeline (Pintaldi et al. 2021; Murphy et al. 2021) to search for highly variable radio sources.

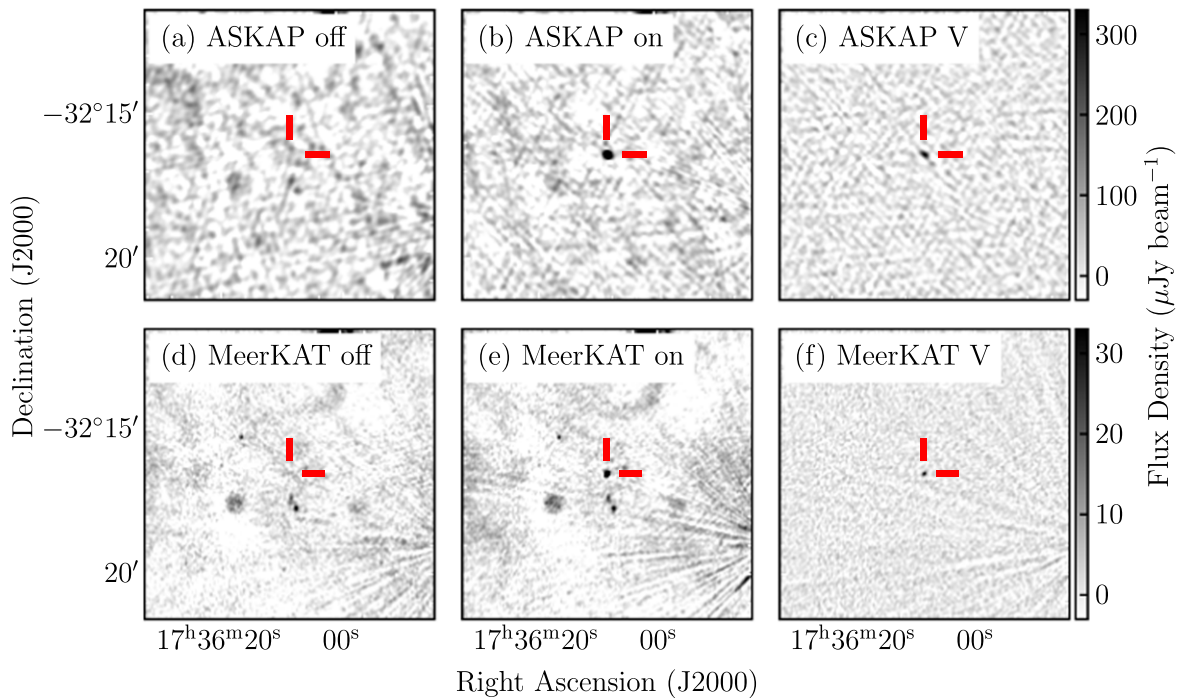[19] https://vast-survey.org/

Figure 1. Upper panels: ASKAP images of ASKAP J173608.2−321635 (centered at 888 MHz). Each image is 10′ on a side, with north up and east to the left. We show the "off" image observed on 2019 April 28 in panel (a), the "on" image observed on 2020 January 11 in panel (b), and Stokes V image from 2020 January 11 in panel (c). The color scales are the same for all of these images. Lower panels: MeerKAT L-band images of ASKAP J173608.2−321635. Each image is 10′ on a side, with north up and east to the left. We show the "off" image observed on 2021 January 19 in panel (d), the "on" image observed on 2021 February 7 in panel (e), and Stokes V image from 2021 February 7 in panel (f). The color scales are the same for all of these images.

Given its high stellar density and ongoing star formation, the Galactic Center (GC) is a promising region for finding variable and transient radio sources (e.g., Lazio et al. 2006). Aside from transients of known origin like X-ray binaries (e.g., Bower et al. 2005; Zhao et al. 2020), 1A 1742–28 (Davies et al. 1976) and the Galactic Center transient (GCT; Zhao et al. 1992) were the first two radio transients detected, and are only ∼arcminutes away from the GC. Three Galactic Center radio transients (GCRTs) were discovered in the 2000 s at lower frequencies: GCRT J1746–2757 (Hyman et al. 2002), GCRT J1745–3009 (Hyman et al. 2005), and GCRT J1742–3001 (Hyman et al. 2009). Unlike A1742–28 and GCT, the GCRTs are about a degree away from the GC, but they are all at low Galactic latitudes ($|b| < 0°.6$). Though the radio properties for these three GCRTs are not identical to each other, the spectra of all three GCRTs are very steep and none of them has a clear counterpart at other wavelengths. The most well-studied of the three, GCRT J1745–3009, was detected in at least two different states: it emitted ∼1 Jy bursts every 77 minutes in 2002, and gave off weaker (∼50 mJy) single bursts in 2003 and 2004. Hyman et al. (2007) suggest that GCRT J1745–3009 likely belongs to a new class of coherent emitters, while most radio transients are incoherent synchrotron sources. Also, there are yet further candidates in need of confirmation and followup (e.g., Chiti et al. 2016).

In this paper we report the discovery of a highly polarized, variable source near the GC, ASKAP J173608.2−321635, detected at 888 MHz in VAST-P1 observations with ASKAP, and redetected at 1.29 GHz with MeerKAT (Jonas 2016; Camilo et al. 2018). We present the observations, including radio imaging, pulsar searching, X-ray searches, and near-infrared imaging in Section 2, and discuss the possible nature of the source in Section 3.

2. Observations, Data Reduction, and Results

2.1. ASKAP Observations

ASKAP J173608.2−321635 was first discovered as a compact radio source in a transients search of VAST-P1 data (Project Code AS107) using the VAST transient detection pipeline (Figure 1). It was detected in the adjacent fields 1724−31A and 1752−31A, observed 13 times between 2019 April 28 and 2020 August 29. The VAST-P1 survey incorporates the Rapid ASKAP Continuum Survey (RACS, Project Code AS110; McConnell et al. 2020) as its first epoch. Both RACS and VAST-P1 were conducted at a central frequency of 888 MHz with a bandwidth of 288 MHz and they shared the same tiling footprints. The integration time for RACS was 15 minutes while that for VAST-P1 was 12 minutes, achieving an rms noise of 0.36 mJy beam^{-1} and 0.40 mJy beam^{-1} for regions near the GC, respectively. Details of these survey observations and data reduction are given by McConnell et al. (2020) and Murphy et al. (2021).

Figure 2 shows the full radio lightcurve of ASKAP J173608.2−321635, as well as the fractional circular polarization. Other than variability, ASKAP J173608.2−321635 was highly circularly polarized with a fractional polarization ranging from 20% to 30% in VAST-P1 bright detections (see Figure 2, lower left panel).

There were four additional ASKAP observations that cover our source (Table 1). These observations were calibrated using PKS B1934–638 for both the flux density scale and the instrumental bandpass. All observations were processed using standard procedures in the ASKAPSOFT package (Guzman et al. 2019). We note that there was a ∼50 mJy detection in a 10-hour observation at 943 MHz on 2020 November 1. However, the systematic error is high due to the source being located near the edge of the beam.
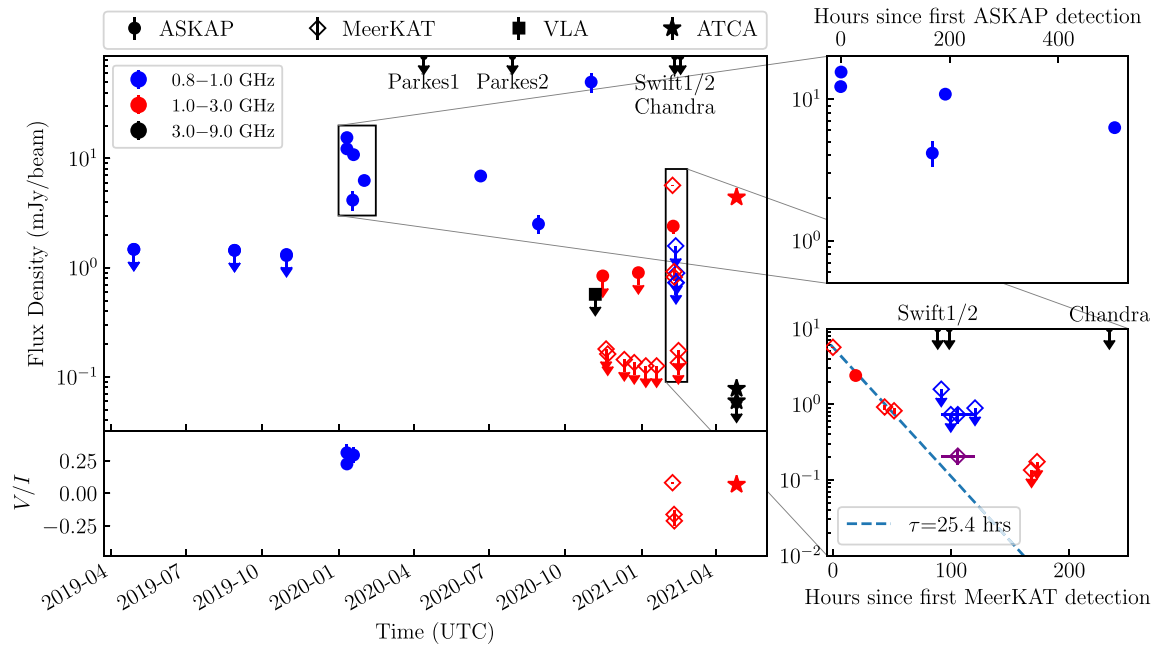
Figure 2. Full radio lightcurve for ASKAP J173608.2−321635, including nondetections (times of X-ray observations are also indicated). The circular polarization fraction V/I is shown in the bottom panel for the detections. In the upper right panel, we show the detections with ASKAP from 2020 January. In the lower right panel, we show the observations close to the MeerKAT detections from 2021 February. We fit an exponential decay of the form $S \propto e^{-t/\tau}$ for the four 1.3 GHz detections (blue dashes line) and find the timescale of decay to be ∼26 hr. We scale the UHF band (800 MHz) detection to the L band (1.3 GHz) with the spectral index $\alpha \sim -2.7$ and show the scaled flux density as the purple diamond.

To check for any shorter timescale variability we imaged the source using data from the 2020 November 1 ASKAP observation with an integration time of 15 min (resulting in 40 images in total). This lightcurve showed a relatively low modulation index (standard deviation divided by the mean) of ∼13%, and had a reduced χ^2 relative to a constant model (a measure of the significance of the variability, see, e.g., Swinbank et al. 2015) of 1.6 for 39 degrees of freedom (40 observations minus one parameter for the mean). Overall we did not see any evidence for hour-scale variability (Figure 3).

2.2. Parkes Observations

Motivated by the possibility that ASKAP J173608.2−321635 is a pulsar, we conducted follow-up observations with the 64 m Parkes telescope of ASKAP J173608.2−321635 on 2020 April 20 and 2020 July 29 using the pulsar searching mode with the Ultra-Wideband Low (UWL) receiver (Hobbs et al. 2020), which provides simultaneous frequency coverage from 704 to 4032 MHz. Each observation was 30 minutes with 32 μs time resolution and high frequency resolution (1024 channels per 128 MHz subband). We used PRESTO (Ransom 2001) to perform a standard pulsar search. We found no candidates in a search of dispersion measures (DMs) spanning 0–3000 pc cm^{-3}, corresponding to 25 kpc based on the YMW16 electron-density model (Yao et al. 2017, hereafter YMW16) or about two times the highest DM for pulsars discovered to date (e.g., Shannon & Johnston 2013), period <25 s and accelerations up to ∼20 m s^{-2} (assuming a pulsation period of 1 ms). We also found no single pulse above a signal-to-noise ratio (S/N) of 8 using the single pulse search procedure for PRESTO. However, the lack of simultaneous imaging meant we cannot determine whether the source was radio-loud during these observations. These nondetections (with an upper limit of ∼0.05 mJy, assuming the

duty cycle of the pulsar (W/P) to be 10%) therefore do not rule out the presence of a pulsar.

2.3. MeerKAT Observations

To simultaneously search for pulsed and continuum emission from ASKAP J173608.2−321635, we observed it using the MeerKAT radio telescope with a central frequency of 1.28 GHz and a two-week cadence starting from 2020 November 19 (project code DDT-20201005-DK-01). Each observation had 12 minutes on the target, achieving an rms noise of 40 μJy beam^{-1}. Imaging and pulsar searching were performed simultaneously in all MeerKAT observations. We used PKS J1830–3602 for bandpass, flux density scale and phase calibration. We reduced the image data using OXKAT[20](v1.0; Heywood 2020), where the Common Astronomy Software Applications (CASA; McMullin et al. 2007) package and TRICOLOUR[21] were used for measurement sets splitting, cross calibration, self-calibration, and flagging, and WSCLEAN (Offringa et al. 2014) was used for continuum imaging.

We did not detect any source to a 5σ limit of 0.04 mJy in the first five epochs. However, we detected a source in our observation on 2021 February 7 at a flux density of 5.67 ± 0.04 mJy but did not detect any pulsations. The best-fit position of the source is: (J2000) R.A. $17^h36^m08^s19 \pm 0^s03$, decl. $-32°16'35''0 \pm 0''3$ with Galactic coordinates $l, b = (356°.08, -0°.04)$ based on the MeerKAT detection, where the uncertainties are based on a comparison of the positions of field sources to their RACS matches. We imaged the source with an integration time of 16 s (resulting in 40 images in total). The lightcurve showed a relatively low modulation index of

---

3

Table 1
Radio Observation Summary for ASKAP J173608.2−321635

Telescope	Mode	Start (UT)	Duration (h)	Frequency Range (MHz)	S_{StokesI} (mJy/beam)	S_{StokesV} (mJy/beam)	Survey
VLA	Imaging	1996 May–1996 Jun	⋯	1363–1447	<1.71	⋯	NVSS
Molonglo	Imaging	1997 Jul–2007 May	∼11	841.5–844.5	<15.6	⋯	MGPS-2
MWA	Imaging	2014 Jun	⋯	170–231	<1800	⋯	GLEAM
GMRT	Imaging	2016 Mar	⋯	140–156	<27.0	⋯	TGSS
EVLA	Imaging	2018 Feb 11 15:47	⋯	2000–4000	<0.36	⋯	VLASS
ASKAP	Imaging	2019 Apr 28 20:47	0.25	744–1032	<1.47	⋯	RACS
ASKAP	Imaging	2019 Apr 28 21:03	0.25	744–1032	<1.47	⋯	RACS
ASKAP	Imaging	2019 Aug 28 10:01	0.2	744–1032	<1.44	⋯	VAST-P1
ASKAP	Imaging	2019 Aug 28 11:04	0.2	744–1032	<1.44	⋯	VAST-P1
ASKAP	Imaging	2019 Oct 30 04:02	0.2	744–1032	<1.32	⋯	VAST-P1
ASKAP	Imaging	2019 Oct 30 04:14	0.2	744–1032	<1.39	⋯	VAST-P1
ASKAP	Imaging	2020 Jan 11 02:14	0.2	744–1032	12.24 ± 0.89	3.80 ± 0.77	VAST-P1
ASKAP	Imaging	2020 Jan 11 02:56	0.2	744–1032	15.51 ± 0.48	3.48 ± 0.32	VAST-P1
ASKAP	Imaging	2020 Jan 18 02:56	0.2	744–1032	4.15 ± 0.86	<2.19	VAST-P1
ASKAP	Imaging	2020 Jan 19 02:27	0.2	744–1032	10.82 ± 0.85	3.17 ± 0.66	VAST-P1
ASKAP	Imaging	2020 Feb 01 01:31	0.2	744–1032	6.28 ± 0.47	<1.14	VAST-P1
Parkes	Pulsar	2020 Apr 12 20:50	0.5	704–4032	<0.05[a]	⋯	
ASKAP	Imaging	2020 Jun 20 14:17	0.25	744–1032	6.90 ± 0.35	<0.99	VAST-P1
Parkes	Pulsar	2020 Jul 29 12:29	0.5	704–4032	<0.05[a]	⋯	
ASKAP	Imaging	2020 Aug 29 09:46	0.2	744–1032	2.51 ± 0.49	<1.11	VAST-P1
ASKAP	Imaging	2020 Nov 01 02:16	10	799–1087	∼50 ± 10[b]	⋯	
EVLA	Imaging	2020 Nov 06 20:42	0.5	2000–4000	<0.57	⋯	VLASS
ASKAP	Imaging	2020 Nov 15 06:10	0.25	1295–1439	<0.18	⋯	RACS-mid
MeerKAT	Imaging&Pulsar	2020 Nov 19 14:45	0.2	856–1712	<0.18	⋯	
MeerKAT	Imaging&Pulsar	2020 Nov 21 16:04	0.2	856–1712	<0.16	⋯	
MeerKAT	Imaging&Pulsar	2020 Dec 11 12:15	0.2	856–1712	<0.14	⋯	
MeerKAT	Imaging&Pulsar	2020 Dec 23 09:09	0.2	856–1712	<0.14	⋯	
ASKAP	Imaging	2020 Dec 28 04:09	0.25	1295–1439	<0.90	⋯	RACS-mid
MeerKAT	Imaging&Pulsar	2021 Jan 06 10:05	0.2	856–1712	<0.12	⋯	
MeerKAT	Imaging&Pulsar	2021 Jan 19 09:13	0.2	856–1712	<0.12	⋯	
MeerKAT	Imaging&Pulsar	2021 Feb 07 06:09	0.2	856–1712	5.67 ± 0.04[c]	0.46 ± 0.03	
ASKAP	Imaging	2021 Feb 08 01:23	0.25	1295-1439	2.40 ± 0.33	⋯	RACS-mid
MeerKAT	Imaging&Pulsar	2021 Feb 09 01:55	0.2	856–1712	0.92 ± 0.06[d]	−0.15 ± 0.03	
MeerKAT	Imaging&Pulsar	2021 Feb 09 09:59	0.2	856–1712	0.82 ± 0.07[d]	−0.18 ± 0.03	
MeerKAT	Imaging&Pulsar	2021 Feb 11 01:45	0.2	544–1088	<1.56[e]	⋯	
MeerKAT	Imaging&Pulsar	2021 Feb 11 09:50	0.2	544–1088	<0.73[e]	⋯	
MeerKAT	Imaging&Pulsar	2021 Feb 12 06:19	0.2	544–1088	<0.89[e]	⋯	
MeerKAT	Imaging&Pulsar	2021 Feb 14 06:09	0.2	856–1712	<0.13	⋯	
MeerKAT	Imaging&Pulsar	2021 Feb 14 10:49	0.2	856–1712	<0.18	⋯	
ATCA	Imaging	2021 Apr 25 13:37	1.3	4500–6500	<0.078	⋯	
ATCA	Imaging	2021 Apr 25 13:37	1.3	8000–10000	<0.060	⋯	
ATCA	Imaging	2021 Apr 25 14:03	1.3	1100–3100	4.41 ± 0.14[f]	0.29 ± 0.05	

Notes. Nondetections are denoted by 3σ upper limits based on the local noise
[a] The upper limit is derived from Equation (1). We assumed the duty cycle of the pulsar (W/P) to be 10%.
[b] The location of the source is close to the edge of the primary beam. The systematic error can be as high as ∼ 10 mJy.
[c] The spectral index across the bandpass is $\alpha = -2.7 \pm 0.1$. RM is -11.8 ± 0.8 rad m^{-2} after ionospheric RM correction.
[d] The spectral index across the bandpass is $\alpha = -3.4 \pm 0.3$. RM is -64.0 ± 1.5 rad m^{-2} after ionospheric RM correction.
[e] We combined these three UHF observations and got a detection with flux density of 0.73 ± 0.17 mJy beam^{-1}.
[f] The spectral index across the bandpass is $\alpha = -5.6 \pm 0.3$.

∼4% and had a reduced χ^2 of 0.8 for 39 degrees of freedom, with no evidence for minute-scale variability (Figure 3).

The source was moderately circularly polarized ($V/I = +8\%$) and had a steep radio spectrum within the bandpass ($\alpha = -2.7 \pm 0.1$[22], where $S_\nu \propto \nu^\alpha$). We also found the source to be highly linearly polarized ($|L|/I \sim 80\%$) with a moderately

low Faraday rotation measure (RM) of -11.2 ± 0.8 rad m^{-2}. The source also exhibited depolarization behavior toward lower frequencies: the fractional total polarization is nearly 100% at 1.6 GHz but only ∼20% at 0.9 GHz (Figure 4). We performed further tests to verify the polarization and RM variability, as discussed in the Appendix.

Further radio observations showed a very rapid decline with an exponential timescale of ∼26 hr (Figure 2 inset). Our ASKAP observation 20 hr after the first MeerKAT detection

---

[22] Subband calibration has not been properly evaluated, and hence we are aware that our estimates may include ∼10% calibration error.
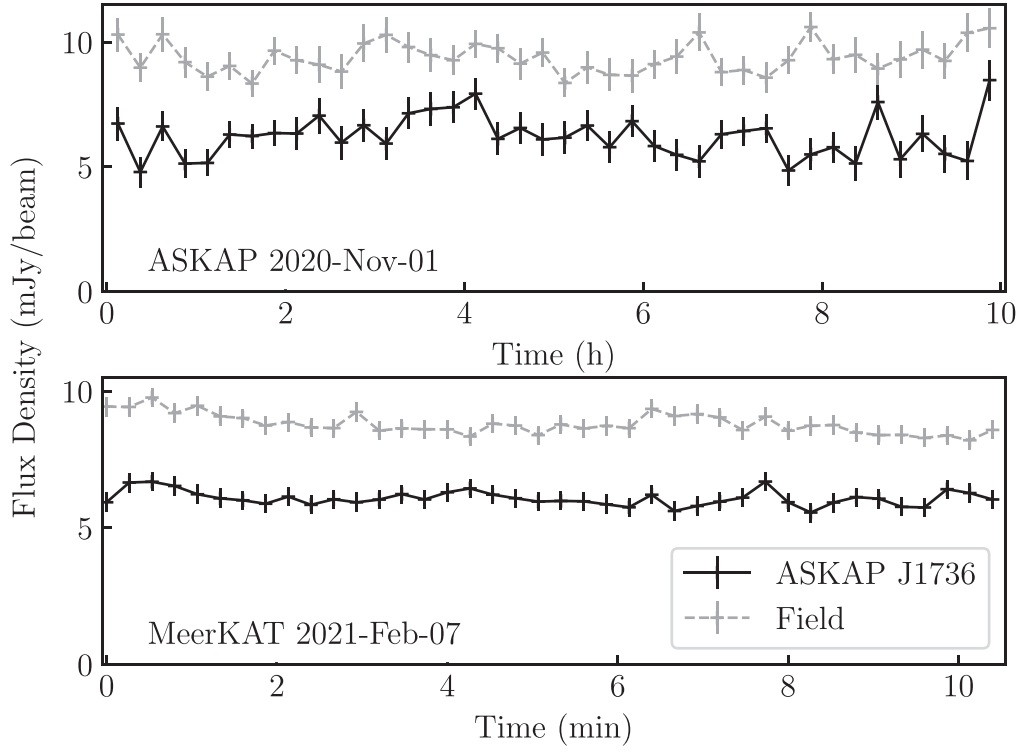
Figure 3. Short-timescale lightcurves for ASKAP J173608.2−321635. Top: The observation on 2020 November 1 using ASKAP. The integration time for each point is 15 min. Bottom: The observation on 2021 February 7 using MeerKAT. The integration time for each point is 16 s. The black solid lines are lightcurves for ASKAP J173608.2−321635 and the gray dashed lines are lightcurves for a field source (J173548.2−310811) as a comparison.
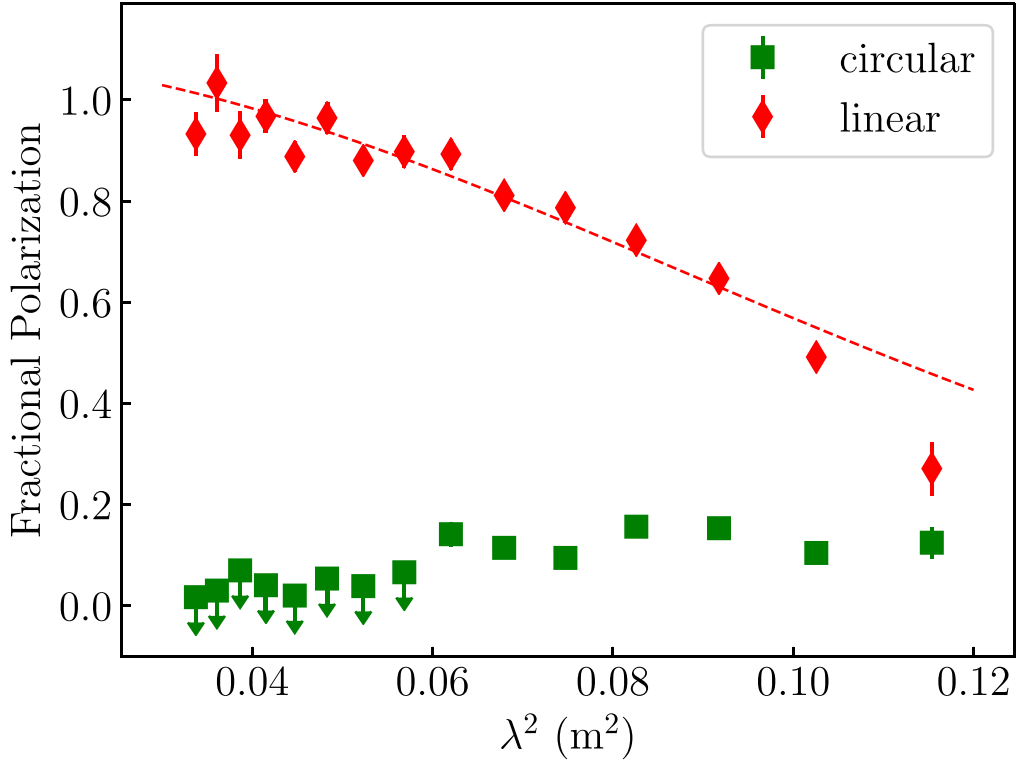

Figure 4. Fractional polarization as a function of λ^2 in the MeerKAT L-band observation taken on 2021 February 7. We show the circular polarization as green squares, and linear polarization as red diamonds. We fit a simple depolarization equation $\Pi = \Pi_0 \exp(-2\sigma^2\lambda^4)$ to the linear polarization data, which is shown as the red dashed line, where $\sigma = 5.7\ \mathrm{m}^{-2}$ is the RM dispersion of the Faraday screen (Farnes et al. 2014).

gave a flux density of 2.4 ± 0.3 mJy at 1.3 GHz. Two further MeerKAT observations over the following days demonstrated that the source continued to fade exponentially, while the spectral shape remained similar ($\alpha = -3.4 \pm 0.3$). We found the source was still highly linearly polarized in these observations, although the RM changed significantly, from

-11.2 ± 0.8 rad m^{-2} on 2021 February 7 to -63.3 ± 1.5 rad m^{-2} on 2021 February 9. The ionosphere usually contributes to Faraday rotation of order ~ 1 rad m^{-2} (Sotomayor-Beltran et al. 2013), which can potentially cause RM variations between epochs. We used IONFR[23] to model the ionospheric Faraday depth at the dates of the observations. The ionospheric Faraday rotation is $+0.65 \pm 0.05$ rad m^{-2} and $+0.75 \pm 0.06$ rad m^{-2} on 2021 February 7 and 2021 February 9, respectively. The corrected RM of the source is therefore -11.8 ± 0.8 rad m^{-2} and -64.0 ± 1.5 rad m^{-2} on these days, after ionospheric RM corrections. The intrinsic polarization angle was consistent between the epochs (see justifications in the Appendix).

We also obtained three 12 minute observations in the ultra-high-frequency band (UHF; 544–1088 MHz) with MeerKAT, about 100 hours after the first MeerKAT detection. There was no detection in these single observations, but there was a $\sim 5\sigma$ detection when all three were summed coherently (see blue diamonds in Figure 2). This UHF-band detection is a factor of two higher than what we expected from the exponential decay (we corrected the UHF-band detection to 1.3 GHz assuming a spectral index of $\alpha = -2.7$), suggesting that the spectrum may have steepened to $\alpha < -4$ or that the decay slowed.

During imaging observations with MeerKAT, the FBFUSE (Filterbanking Beamformer User Supplied Equipment; Barr 2017) instrument was used to produce high-time-resolution Stokes-I beams to enable pulsar and fast-transient searching. At both the L and UHF band, FBFUSE was configured to produce a tiling pattern of seven coherent beams with the central beam positioned at (J2000) R.A. $17^{\rm h}36^{\rm m}08\overset{\rm s}{.}20$, decl. $-32°16'33\overset{''}{.}0$. The beams were arranged in a close-packed hexagonal grid with an overlap at their 70% power points (see Chen et al. 2021 for detail of FBFUSE beam tiling). At the L band FBFUSE produced 4096-channel data covering the 856 MHz band with a time resolution of 76.56 μs. At the UHF band the instrument produced 4096-channel data covering the 544 MHz band with a time resolution of 120.47 μs.

Data streams from FBFUSE were recorded to disk on the Accelerated Pulsar Search User Supplied Equipment (APSUSE; Barr 2017) cluster. The data were dedispersed to dispersion measures in the range 0–2000 pc cm^{-3} at the UHF band and 0–3000 pc cm^{-3} at the L band, with the different maximum DMs chosen to have roughly constant scattering timescales between the two bands. The resultant trials were searched for periodicities up to 10 s using the GPU-accelerated PEASOUP[24] software with the resultant candidates folded modulo the detected periodicities using PULSARX.[25] To retain sensitivity to binary systems, the data were time-domain resampled (Johnston & Kulkarni 1991) to constant acceleration values between -150 and 150 m s^{-2} before searching. Folded candidate signals were inspected by eye. No significant pulsed emission was detected above a signal-to-noise threshold of 9.

The MeerTRAP real-time single-pulse pipeline running on the Transients User Supplied Equipment (TUSE) instrument (B. W. Stappers et al. 2021, in preparation) was run in parallel with all of the MeerKAT observations. It operated on the same central beam that the pulsar search described above with a time resolution of 306.24 μs for the L-band observations and 361.4 μs for the UHF-band observations. Single pulses that are greater than an S/N limit of 8 were searched for

---
23 https://github.com/csobey/ionFR
24 https://github.com/ewanbarr/peasoup
25 https://github.com/ypmen/PulsarX.git

overdispersion measures from 23–5000 pc cm^{-3} in the L band and 23–1500 pc cm^{-3} in the UHF band over a range of widths from the time resolution up to 196 ms and 231 ms for the two frequencies, respectively. No astrophysical pulses were detected above the S/N threshold.

2.4. ATCA Observations

After our ASKAP and MeerKAT monitoring observations ended, we observed ASKAP J173608.2$-$321635 with the Australia Telescope Compact Array (ATCA) in three bands (centered at 2.1 GHz, 5.5 GHz, and 9.0 GHz) for 80 minutes each on 2021 April 25 (project code: C3431). The observation was calibrated using PKS B1934$-$638 for the flux density scale and the instrumental bandpass. PMN J1733$-$3722 was used for phase calibration.

We used MIRIAD (Sault et al. 1995) to perform the data calibration and CASA to perform the continuum imaging. We detected a source with a flux density of 4.41 ± 0.14 mJy at 2.1 GHz. We did not find any detection at 5.5 GHz or 9.0 GHz, which places 3σ upper limits of 78 μJy beam^{-1} and 60 μJy beam^{-1} at 5.5 GHz and 9.0 GHz, respectively. The nondetection at higher frequency (5.5 GHz) constrains the spectral index to be $\alpha < -4.2$. We measured the spectral index to be $\alpha = -5.6 \pm 0.1$ across the L-band (2.1 GHz) bandpass (Figure 5), which is consistent with the constraints from the nondetection at 5.5 GHz. The source was moderately circularly polarized, with $V/I \sim +6\%$, which is consistent with the MeerKAT observation that fractional circular polarization is lower at higher frequencies (Figure 4).

2.5. X-Ray Observations and Analysis

We identified archival observations covering ASKAP J173608.2$-$321635 with the Neil Gehrels Swift Observatory (Swift; Gehrels et al. 2004), restricting observations to those using the X-Ray Telescope (XRT; Burrows et al. 2005) in the photon counting mode. We used four observations between 2012 February 1 and 2012 September 9, with a summed exposure time of 2.3 ks. There was no source within 15$''$ of ASKAP J173608.2$-$321635, and we determine a 95% count-rate upper limit of 8.4×10^{-4} s^{-1} (over the default energy range of 0.2–10 keV).

Following the MeerKAT detections of ASKAP J173608.2$-$321635, we were awarded Director's Discretionary Time observations with Swift (observation IDs 00014071001 and 00014071002). We obtained 1.7 ks on 2021 February 10.95 and another 0.8 ks on 2021 February 11.35. There was one count within 15$''$ of ASKAP J173608.2$-$321635, but this is consistent with the background (mean expectation with 15$''$ of 0.3 counts). So, we set an upper limit of 1.2×10^{-3} s^{-1} (0.2–10 keV). We estimated the upper limit of H I column density for the position of our source based on the H I 4π survey (HI4PI Collaboration et al. 2016) using the HEASARC web-based PIMMS to be 1.59×10^{22} cm^{-2} (through the entire Galaxy). Assuming a power-law photon index of $\Gamma = 2.0$ (Hyman et al. 2021), the nondetection in Swift observations yields an upper limit on the unabsorbed flux (0.3–8 keV) of 2.0×10^{-13} erg cm^{-2} s^{-1}. The upper limit for the X-ray luminosity at a distance of d is $\sim 2.4 \times 10^{33}(d/10\,{\rm kpc})^2$ erg s^{-2}.

Finally, we were awarded Director's Discretionary Time with the Chandra X-Ray Observatory. We used the back-illuminated
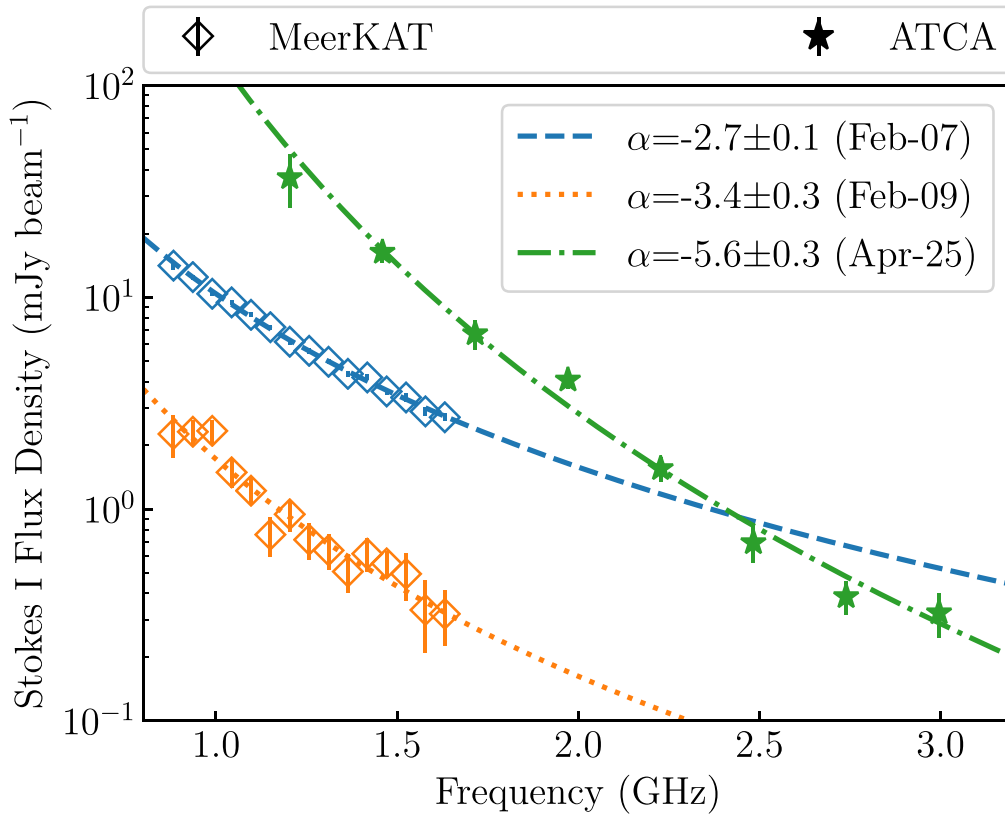
Figure 5. Stokes I spectral energy distributions for ASKAP J173608.2−321635 from two observations with MeerKAT (0.9–1.6 GHz; diamonds) and one with ATCA (1.4–3.0 GHz; stars). We fit a power law relation for each observation and show the spectral index and the date of the observation in the legend.

ACIS-S3 detector with the thin filter, and the 1/8 subarray to maintain subsecond temporal resolution. ASKAP J173608.2−321635 was observed on 2021 February 17.61 for 25.1 ks (observation ID 24966). We filtered the data to 0.3–10 keV. There are 0 events within $1''$, and based on the observed background rate we set a 95% upper limit of $1.0 \times 10^{-4}\,\mathrm{s}^{-1}$. Likewise, we estimate the upper limit of the X-ray luminosity (0.3–8 keV) based on the Chandra nondetection to be $\sim 5.0 \times 10^{31}(d/10\,\mathrm{kpc})^2$ erg s^{-1}.

2.6. Near-infrared Data

We searched for near-IR counterparts in the VISTA Variable in the Via Lactea Survey (VVV; Minniti et al. 2010). There is no counterpart visible in the VVV DR2 catalog. We find 3σ upper limits of $J > 19.25$, $H > 17.65$ mag, and $K_s > 16.70$ mag from VVV within a $2''5$ radius (corresponding to a 5σ positional error).

We observed the source using Gemini Flamingos-2 in the J-band (1.2 μm) for 40 minutes on 2021 April 28 and 2021 April 29, and in the K_s band (2.15 μm) for 18.5 minutes on 2021 May 24 (project code GS-2021A-FT-210). We used Gemini DRAGONS (Labrie et al. 2019) to reduce the data and SEXTRACTOR (Bertin & Arnouts 1996) to perform the photometry.

We used the VVV catalog as both astrometric and photometric references to correct the Gemini data. For astrometry, we used 340 sources that we identified as not blended or badly saturated for the J band and 96 sources for the K_s band. The uncertainty is $\approx 0.15''$ in each coordinate. For photometry, we used fewer sources to avoid sources that showed signs of saturation or nonlinearity. We used 270 sources in the J band and 90 sources in the K_s band. We estimated zero-point uncertainties of 0.02 mag for the J band

and 0.04 mag for the K_s band. The seeing of both observations was $\sim 0''7$.

There is a faint source within $2''5$ of the radio position with $J = 20.8 \pm 0.2$ mag and $K_s = 17.6 \pm 0.1$ mag. This infrared source is just within the 5σ error circle of the radio position (Figure 6), therefore we consider it unlikely to be associated with the radio source, but we examine this in more detail in Section 3.1. Finally, just to the south of that source is a fainter source visible in both J and K_s bands but with magnitudes at or fainter than our 3σ limit. We are unable to measure its properties reliably, but given the density of such sources in the image we do not believe the association to be significant.

2.7. Archival Radio Data

This source was not detected in previous radio surveys including the quick look images from the Karl G. Jansky Very Large Array Sky Survey (VLASS; Lacy et al. 2020), the TIFR GMRT Sky Survey (TGSS; Intema et al. 2017), the GaLactic, and Extragalactic All-sky MWA (GLEAM; Wayth et al. 2015; Hurley-Walker et al. 2017), the NRAO VLA Sky Survey (NVSS; Condon et al. 1998), and the second epoch Molonglo Galactic Plane Survey (MGPS-2; Murphy et al. 2007). These limits are included in Table 1. We have also searched for any archival VLA and ATCA data but did not find any other observation that covers our source.

3. Discussion

We can summarize the most important characteristics of ASKAP J173608.2−321635 before we discuss interpretations:
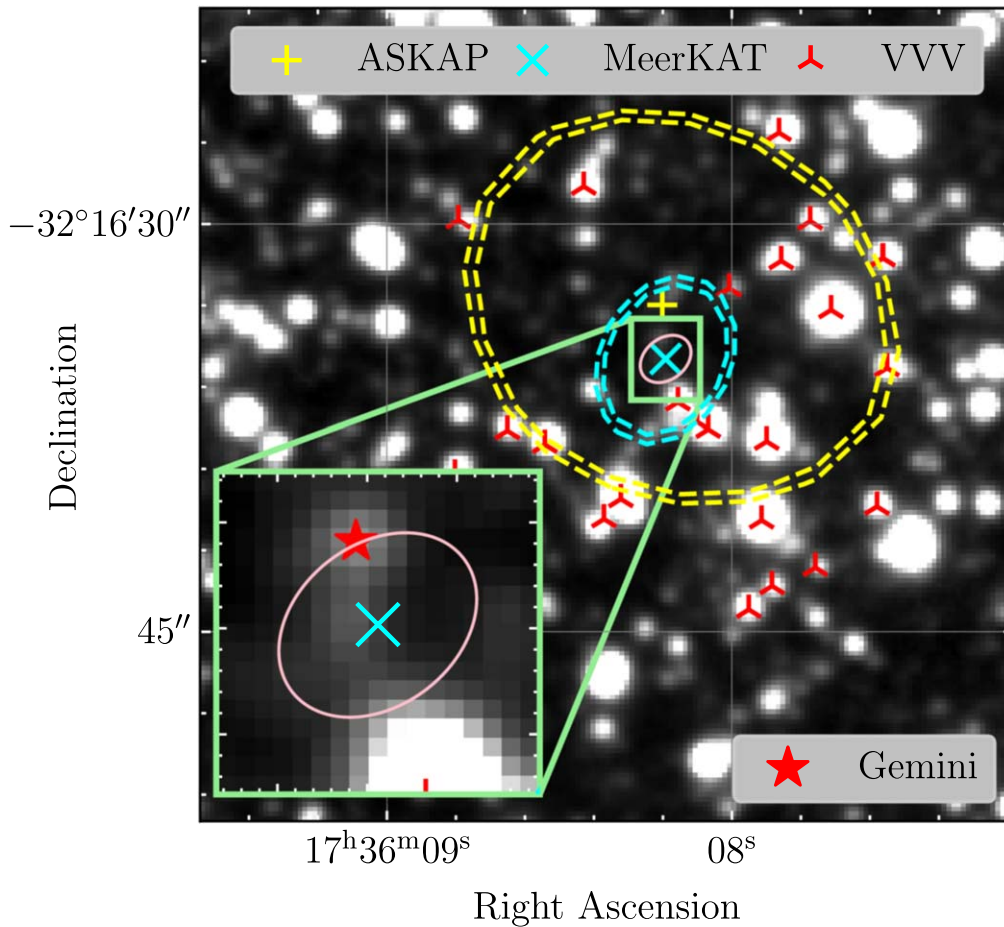
Figure 6. The Gemini J-band (1.2 μm) image (30$''$ on a side, $\sim$2 times the ASKAP synthesized beam) of ASKAP J173608.2−321635. The yellow contours show the ASKAP detection, while the cyan contours show the MeerKAT detection. The best-fit positions from ASKAP and MeerKAT are shown as yellow + and cyan × symbols, respectively. Red inverted Y symbols show the sources from the VVV catalog (Minniti et al. 2010). The small pink contour is the best astrometry constraint from MeerKAT (at 5σ confidence level). We show one well-detected source from Gemini observations that is within 2$''$5 of the radio position as the red star in the inset; there is a fainter source just to the south of that, but it is consistent with our upper limits.

1. Factor of $>$100 variability over a timescale of a week at 900 MHz with a peak flux density of $\sim$10 mJy.
2. Persistent emission for a few weeks, but can decline as fast as 1 day.
3. High degree of circular polarization and steep radio spectrum.
4. High degree of linear polarization with a small RM, and depolarization toward the lower frequencies. RM changes significantly across the observations within three days.
5. No radio pulsations (searching the DM from 0–3000 pc cm^{-3} and exploring the acceleration up to 150 m s^{-2}).
6. No counterpart at near-infrared (down to $J = 20.8$ mag and $K_s = 17.6$ mag) or X-ray wavelengths (with upper limits of $\sim$5.0 $\times$ 10^{31} erg s^{-1}).

Based on its low RM, ASKAP J173608.2−321635 may be a Galactic source. We show the pulsars with known RM and DM within 2° of the source from the ATNF pulsar catalog (Manchester et al. 2005)[26] and extragalactic sources with known RM within 2° from RMTable[27] (v0.1.8, C. Van Eck et al. 2021, in preparation) in Figure 7. The absolute values of the RMs for almost all nearby sources are much higher than

that for our source. Furthermore, according to Hutschenreuter et al. (2021), the RM toward the direction of the source is $\sim$+450 rad m^{-2}, mainly contributed by the Milky Way. If we assume the source is extragalactic, a low RM for our source would require a large $\sim$−450 rad m^{-2} additional contribution to cancel the Galactic RM.

The shortest rise and decay timescales we can constrain for our source are $\tau \sim 1$ day, based on the factor of $\sim$2 rise between 2020 January 18 and 2020 January 19 and the $\sim$day-long decay following the MeerKAT detection on 2021 February 7, although the rise in particular is only weakly constrained . If we assume that the emitting region is less than $c\tau$ in size, then the brightness temperature of our source is $T_B \sim 10^{12}$ K$(d/1$ Mpc$)^2$. The low RM for our source suggests that it is nearby, with $d \lesssim 10$ kpc. If there is not any shorter timescale variability, we can constrain that $T_B \lesssim 10^8$ K, which is far lower than the limit for coherent emission, $\sim$10^{12} K (Readhead 1994). However, this limit cannot help us discriminate between coherent and incoherent source, as some coherent emission can have brightness temperature well below 10^{12} K (e.g., type II, III solar bursts, Reid & Ratcliffe 2014). Even so, the high degree of circular polarization suggests some coherent process such as electron cyclotron maser emission may be operating (e.g., Dulk 1985; Pritchard et al. 2021, and see below).

---

[26] http://www.atnf.csiro.au/research/pulsar/psrcat
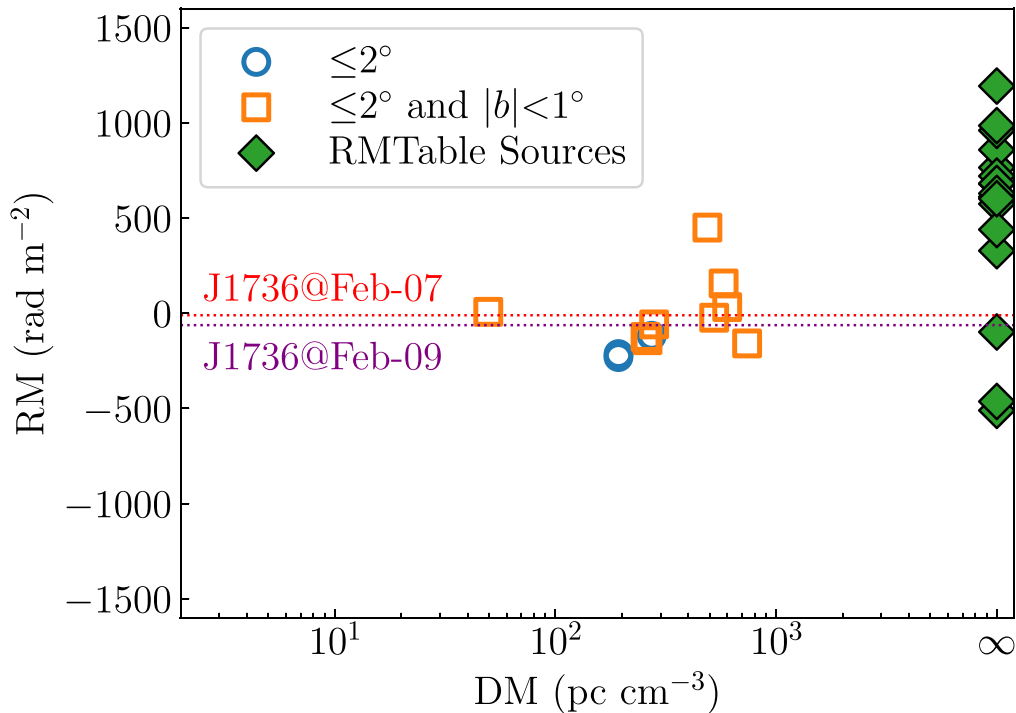[27] https://github.com/CIRADA-Tools/RMTable

Figure 7. Dispersion measure (DM) vs. rotation measure (RM) for pulsars within 2° of the ASKAP J173608.2−321635 from the ATNF pulsar catalog (Manchester et al. 2005). Orange squares show pulsars near the Galactic Plane ($|b| < 1°$) and blue circles show pulsars at higher latitudes. We also show sources within 2° of the source from the RMTable catalog (C. Van Eck et al. 2021, in preparation) as green diamonds (we plot them with DM = ∞ as most of them are extragalactic). The red and purple dashed lines show the RMs from our observations on 2021 February 7 and 2021 February 9, respectively.

Significant changes in rotation measure as seen for ASKAP J173608.2−321635 are rare. Sources with short timescale RM variations are usually extragalactic, such as AGNs with extreme environments (e.g., Zavala & Taylor 2003; Lico et al. 2017; Anderson et al. 2019), and some fast radio bursts (FRB 121102, Hilmarsson et al. 2021). RM variations for Galactic sources are usually slow and small (e.g., Yan et al. 2011; Wahl et al. 2021) except the GC magnetar PSR J1745−2900: Desvignes et al. (2018) found large changes in observed RM for PSR J1745 −2900 by up to 3500 rad m^{-2} over four years. Even more interestingly, they found that the RM for PSR J1745–2900 changed by about 7.4 rad m^{-2} per day in 2017. The RM variations is thought to come from a minimum scale of magneto-ionic fluctuations in the scattering screen.

As we see no change in the intrinsic polarization angle for our source (Appendix), we infer that the RM variation for ASKAP J173608.2−321635 is not intrinsic to the source but is probably external, related to a change in the intervening interstellar medium (ISM). With only two RM measurements, it is hard to put a strong constraint on the property of the ISM along the line of sight. However, given the observational features of ASKAP J173608.2−321635, we can still describe the medium as well as the source more broadly.

Based on the typical magnetic field values for interstellar medium (Ferrière 2001; Han 2017), the length scale of the Faraday region to give the change in RM is $l_{RM} \sim 250 \, \mathrm{pc} (B/2 \, \mu G)^{-1}(n_e/10^{-1} \, cm^{-3})^{-1}$, where B is the magnetic field and n_e is the electron density of the interstellar medium. Since we see no turnover in our radio spectrum, this suggests that the turnover frequency should be lower than ~ 1 GHz if the source is a synchrotron emitter, which means the magnetic field of the source is $\lesssim 3 \times 10^4$ G (e.g., Kellermann & Pauliny-Toth 1981): which is consistent with the argument above but not

very constraining; moreover, the high degree of circular polarization suggests that this is not typical synchrotron emission. The optical depth of free–free absorption at the frequencies we observed should be much smaller than one, which implies $n_e \ll 10^2 \, cm^{-3}(T/10^4 \, K)^{0.675}(l_{abs}/250 \, pc)^{-0.5}$, where T is the temperature and l_{abs} is the length scale of the absorber (e.g., Osterbrock 1989): again, consistent but not necessarily constraining. If we assume there is no change in magnetic field, the RM variation implies a DM variation to be $\sim 30 \, pc \, cm^{-3}(B/2 \, \mu G)^{-1}$ in three days, much higher than those measured in pulsar timing (e.g., You et al. 2007; Demorest et al. 2013; Lam et al. 2018; Donner et al. 2020). It is still high ($\sim 1 \, pc \, cm^{-3} \, yr^{-1}$) even if we assume the magnetic field can be as high as that near the GC (~ 0.8 mG, Eatough et al. 2013).

Only a few types of radio sources are known to emit circular polarization at more than a few percent of their total intensity emission at low frequencies (<5 GHz). These include stars (e.g., Lynch et al. 2017) and pulsars (e.g., Johnston & Kerr 2018). Circular polarization has also been seen from jets in binaries but the fractional polarization is low, $\sim 0.5\%$ (e.g., Fender 2003; Macquart 2003), with similar values seen in extragalactic sources (e.g., Macquart et al. 2003). Indeed, recent circular polarization searches have identified both new pulsars (Kaplan et al. 2019) and the first brown dwarf discovered at radio wavelengths (Vedantham et al. 2020). In this section we discuss these possibilities.

3.1. Stellar Interpretation

Low-mass flare stars and chromospherically-active binaries such as RS CVns often show polarized flares (e.g., Mutel et al. 1987; Zic et al. 2019). We show the color–magnitude diagram for sources within the field of our Gemini observation in
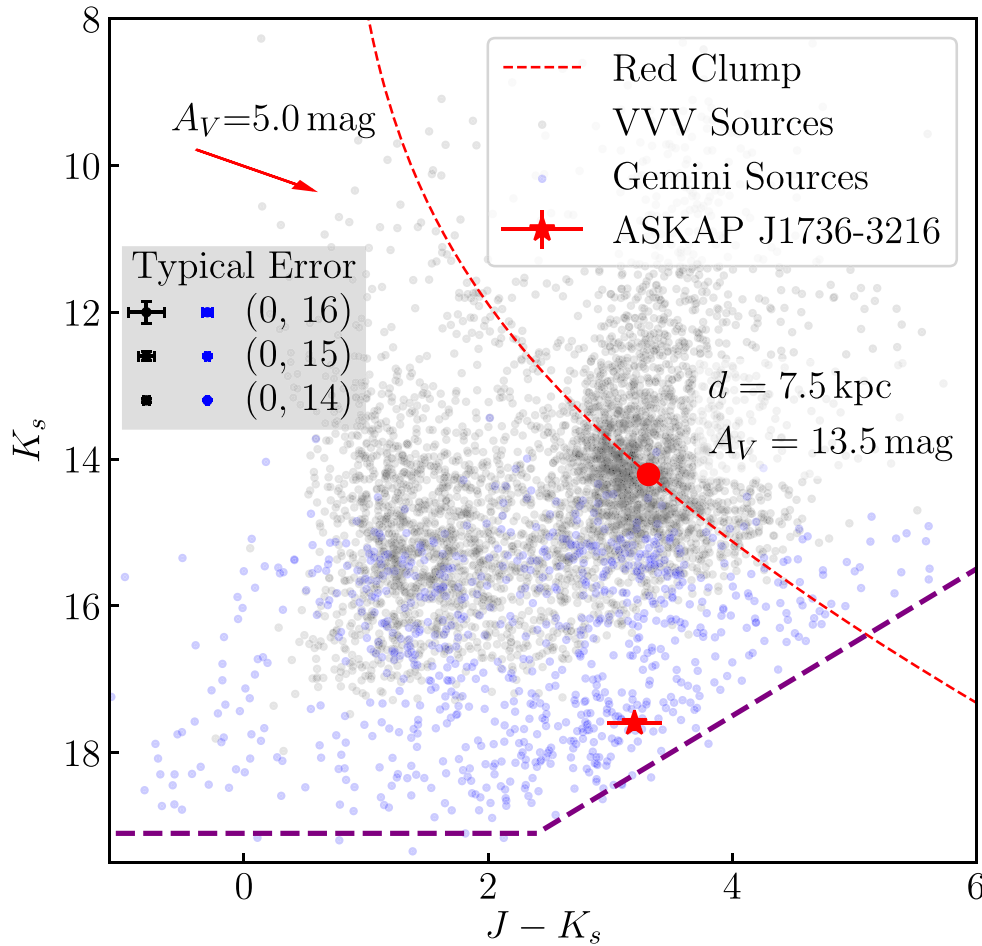
Figure 8. Color-magnitude diagram for the field of ASKAP J173608.2−321635. We plot $J − K_s$ color vs. K_s magnitude. We show sources from VVV and our deeper Gemini observations (both $3'$ in radius) as black dots and blue dots, respectively. The red star shows the possible infrared counterpart candidate of ASKAP J173608.2−321635. We also plot the error for certain pairs of $(J − K_s, K_s)$ values in the center left as a reference. The purple dashed line shows the detection thresholds of our Gemini observation, with $J < 21.5$ mag and $K_s < 19.1$ mag. The red dashed line shows the location of the red clump for different distances. We assume the intrinsic color for the red clump to be $J − K_s = 0.75$ and the intrinsic luminosity $M_K = −1.65$ (Wainscoat et al. 1992; Hammersley et al. 2000). We adopt the extinction coefficients in Yuan et al. (2013) and assume an average extinction in the visual band of $A_V/d ≈ 1.8$ mag kpc^{-1} (Whittet 1992). A reddening vector for $A_V = 5$ mag is also plotted.

Figure 8, with additional sources from VVV. We investigate the possibility that the Gemini source in Figure 6 is a nearby cool dwarf associated with ASKAP J173608.2−321635 (RS CVns would be far brighter, e.g., Driessen et al. 2020). According to Pecaut & Mamajek (2013)[28] cool dwarfs (spectral type of M/L/T/Y) have typical colors of $J − K_s$ from −1.0 to 1.0 and absolute magnitudes in the K_s band of $M_{K_s} \gtrsim 6$. For a cool dwarf with observed color of $J − K_s ≈ 3.0$, it would need at least an extinction in the V band of $A_V ≈ 12$ mag (we use the extinction coefficients in Yuan et al. 2013). With an average extinction of $A_V/d ≈ 1.8$ mag kpc^{-1} (Whittet 1992), it requires a source at a distance of ∼7 kpc, which implies the magnitude in the K_s band would be $\gtrsim 21$ mag (including the effect of extinction). As our source is about 3 magnitudes brighter than this limit, it is hard for this source to be a cool dwarf: more likely is a more distant red giant branch/red clump star. In general it does not stand out at all compared to the surrounding population, suggesting that it is not a unique object. We come to a similar but less robust conclusion about the fainter object

in Figure 6, which we cannot measure reliably (also see Kaplan et al. 2008).

The high radio flux density of ASKAP J173608.2−321635, together with nondetections at X-ray and near-IR wavelengths, also makes a stellar interpretation unlikely. X-ray and radio luminosities for various types of active stars are typically correlated (the Güdel-Benz relation; Güdel & Benz 1993; Driessen et al. 2020). In contrast, ASKAP J173608.2−321635 has an X-ray upper limit too low by at least two orders of magnitude. Even for ultracool dwarfs (known to be radio over-luminous relative to their X-ray luminosity; e.g., Williams et al. 2014), the X-ray limit of our source is lower than most of the ultracool dwarfs (Figure 9).[29]

Similarly, based on the brightest possible object that we cannot rule out in infrared (excluding the object in Figure 6), we measure $J > 20.8$ mag from our Gemini observation. Empirically, we can examine different types of active stars with circularly polarized emission (Figure 10). The vast majority of stars across different types (L/T dwarfs, magnetic CVs, and radio flux-limited samples)
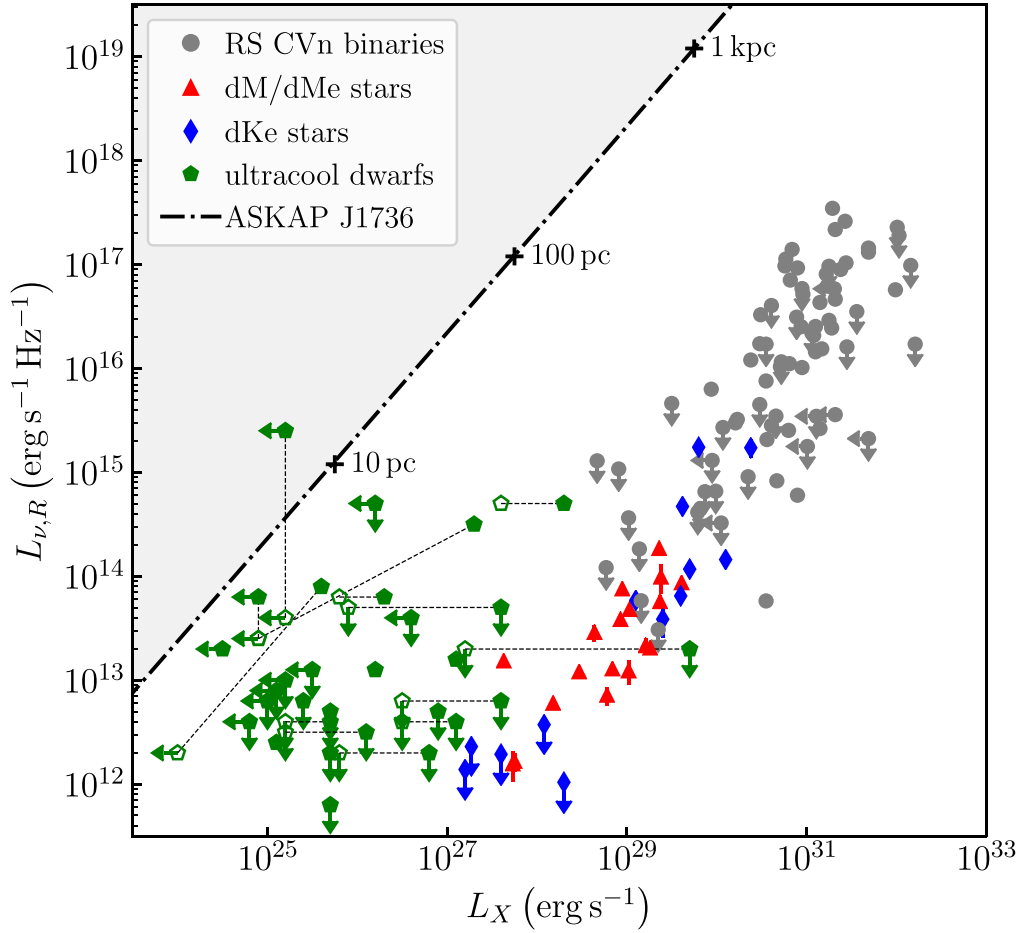

Figure 9. Soft X-ray vs. radio luminosity plot for active stars from Güdel & Benz (1993), Benz & Güdel (1994), Williams et al. (2014), and references therein, adapted from Figure 12 of Driessen et al. (2020). Gray circles are RS CVn binaries, red triangles are *dM/dMe* stars, blue diamonds are *dKe* stars, and green pentagons are ultracool dwarfs. Black dashed lines connect the same source at different states, with the quiescent state shown as hollow markers and flaring state as solid markers. We plot the X-ray luminosity upper limit (0.04–2 keV, based on the model we assumed earlier) for ASKAP J173608.2−321635 at different distances (as labeled) as the black dotted–dashed line, limiting the source to the shaded region to the upper left.

have radio-to-near-IR flux ratios of $\lesssim 1$. For the radio-discovered T dwarf BDR J1750 + 3809, the ratio is near 10. Except for the youngest, most energetic pulsars, this ratio is typically $\gtrsim 10^3$ (e.g., Zyuzin et al. 2016). ASKAP J173608.2−321635 itself has a ratio $> 10^3$, depending on the radio state.

We can do the same analysis a different way, based on the ratio of radio to bolometric flux from ultracool dwarfs. We determined a lower limit on the distance of a stellar/substellar counterpart (spectral type from late L to mid-M) to be ~ 150–1400 pc based on the observed population of ultracool dwarfs (Reid et al. 2008). At this distance, we would expect low extinction, about 0.5 mag in the J band. Based on this lower limit on the distance (applying the extinction correction), we calculated upper limits on the radio flux density at 888 MHz to be < 0.3–0.6 μJy, assuming $L_{\rm radio}/L_{\rm bol} = 10^{-7}$ (which is the typical value for M dwarfs, see Berger et al. 2010). The ratio of radio luminosity to bolometric luminosity for later L dwarfs can be as high as 10^{-5}: for BDR J1750 + 3809, it can reach 2×10^{-5}. The limit would give an expected radio flux density of < 120 μJy. Even for a slightly beamed emission (such as for Jupiter, Burningham et al. 2016), the expected flux density would be $\lesssim 0.9$ mJy. This is considerably lower than our measured values of ~ 10 mJy, suggesting that ASKAP J173608.2−321635 is either a star with an extreme near-IR to radio ratio or another kind of source entirely.

To summarize, we excluded ASKAP J173608.2−321635 as a star based on the following:

1. Compared to its color ($J - K_s$), the IR source that we detect is too bright in the K_s band (Figure 8).
2. The ratio of X-ray luminosity to radio luminosity is too low for stars (Figure 9).
3. The source is too bright in radio compared to the J band (Figure 10).

3.2. Pulsar Interpretation

Though we found no pulsations in our data, the high degree of polarization and steep spectrum suggest the source may be a pulsar. We can use our MeerKAT observations to constrain the pulsar-like properties of ASKAP J173608.2−321635. The expected signal-to-noise ratio of a pulsar at the beam center can be estimated as (Lorimer & Kramer 2012):

$$\mathrm{S/N_{exp}} = \frac{SG\sqrt{N_{\rm pol}\tau_{\rm obs}\Delta\nu}}{T_{\rm sys}\beta}\sqrt{\frac{P-W}{W}}, \qquad (1)$$

where S is the flux density of the pulsar, $G = 2.8$ K Jy^{-1} is the gain of the MeerKAT telescope, $N_{\rm pol} = 2$ is the number of polarizations recorded, $\tau_{\rm obs} = 700$ s is the length of the
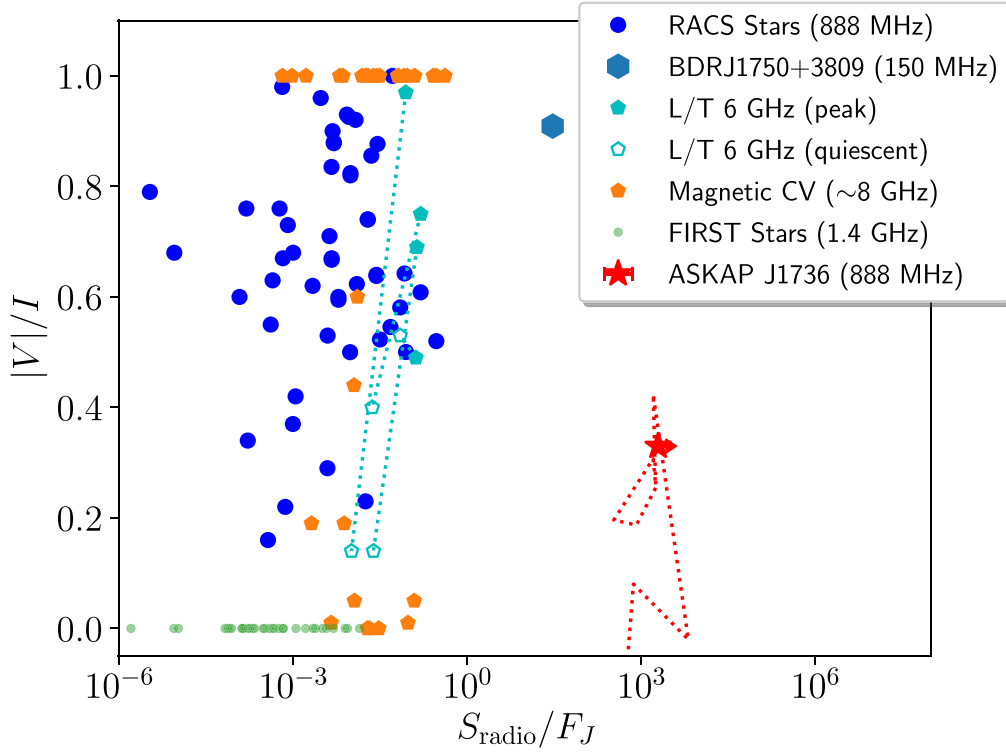
Figure 10. Fractional circular polarization vs. radio-to-near-IR flux ratio for stellar sources. We show stars measured in the Faint Images of the Radio Sky at Twenty Centimeters (FIRST) survey at 1.4 GHz as small green circles (Helfand et al. 1999; no polarization information was available) magnetic CVs measured at 8 GHz as orange pentagons (Barrett et al. 2020), auroral emission from L/T dwarfs measured at 6 GHz as the cyan pentagons for quiescence (open symbols) and peak (filled symbols; Kao et al. 2016), the T dwarf BDR J1750 + 3809 measured at 150 MHz as the blue hexagon (Vedantham et al. 2020), and stars identified in RACS as blue circles (Pritchard et al. 2021). ASKAP J173608.2−321635 is the large red star. When available, dashed lines connect different radio states for the same source. The near-infrared data were taken from VVV (Minniti et al. 2010) and the Two Micron All Sky Survey (2MASS; Skrutskie et al. 2006).

observation, $\Delta\nu \sim 856$ MHz is the bandwidth, $T_{sys} \sim 40$ K is the system temperature (which includes the sky temperature in this direction), β is a correction factor due to downsampling, W is the pulse width of the pulsar, and P is the period of pulsar. The effective pulse width is a combination of its intrinsic pulse width, pulse broadening due to dispersion, and scattering:

$$W_e = \sqrt{W^2 + \delta t_{disp}^2 + \delta t_{scat}^2}, \qquad (2)$$

where W_e is the effective pulse width, $\delta t_{disp} = 8.3 \times 10^6 \mathrm{DM} \, \nu_{MHz}^{-3} \, \delta\nu$ ms ($\delta\nu$ is the channel bandwidth in units of MHz) is the smearing time due to dispersion across a channel observed at frequency ν_{MHz}, and δt_{scat} is the smearing time due to scattering. We considered scattering as a function of DM based on Bhat et al. (2004); note that this is consistent with the very high degree of scattering from Camilo et al. (2021).

A wide effective pulse width can reduce the pulsation S/N. For example, Hyman et al. (2021) argues that C1709–3918 and C1748–2827, with steep spectra, 10%–20% circular polarization, but no pulsations detected, may be pulsars with scatter-broadened pulses. At the most conservative, if ASKAP J173608.2−321635 is a pulsar with 1 ms pulsation period, considering the effect of dispersion and scattering, the nondetection in our MeerKAT pulsar search with S/N = 9 threshold suggests that the duty cycle (W/P) of the pulsar would be >99% for a source with a DM below 200 pc cm^{-3} ($\sim$3 kpc based on YMW16). For longer pulse periods we would have a duty cycle limit of >99% at DMs up to $\lesssim$1000 pc cm^{-3} ($\sim$6 kpc based on YMW16). Compared to pulsars in ATNF

pulsar catalog, the highest duty cycle is $\sim$80% (see Figure 11). However, at the highest DMs considered in our search (up to 3000 pc cm^{-3}), we would not be sensitive to even the longest period pulsars with typical scattering behavior. Observing at higher frequencies can help us minimize the effect of scattering. We will also employ fast folding algorithms (Staelin 1969) to search for longer periods when they become available for MeerKAT data.

An alternative way to smear pulsations would be through orbital acceleration in a tight binary (e.g., Maan et al. 2018; de Gasperin et al. 2018). Our MeerKAT searches were shorter than the Parkes observations, so most binary orbits would not be too smeared out. Based on the range of accelerations searched, we exclude pulsars in a binary system with orbital period $P_B \gtrsim 5$ hr (assuming circular edge-on orbit, pulsar mass of 1.4 $M_\odot$, and companion mass of 0.1 $M_\odot$).

The decline in flux seen in our MeerKAT detections (lower right panel of Figure 2) is a factor of >10 faster than the initial detections seen with ASKAP (upper right panel in Figure 2), with several intermediate values between the "high" state and nondetections. This suggests that what we see is not "on versus off" behavior, like might be expected for a standard intermittent pulsar (Kramer et al. 2006; Lyne 2009).

These intermediate flux levels may also rule out effects such as random sampling of eclipses from a "black widow" (e.g., Fruchter et al. 1988) or "redback" (e.g., Roberts 2013) system, where radio pulses can be periodically eclipsed when the companion wind's obscures the line of sight, and this can both smear out pulsations (e.g., Stappers et al. 1996) and block the continuum flux (Broderick et al. 2016; Polzin et al. 2020).
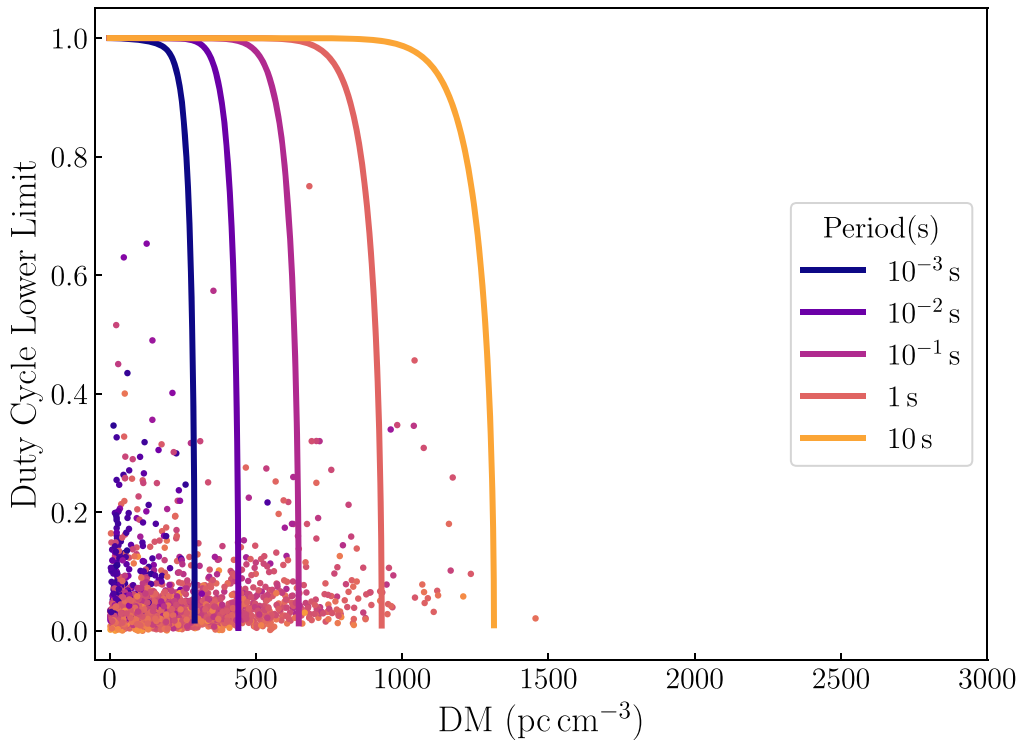
Figure 11. Duty cycle lower limit for a nondetection in the pulsar search for the MeerKAT data from 2021 February 7 (at 856–1712 MHz). We considered pulse broadening effects from dispersion and scattering (Bhat et al. 2004) as a function of DM. We also plot DM vs. duty cycle (width of pulse at 50% peak/period) of the pulsars in the ATNF pulsar catalog (Manchester et al. 2005) with colors to indicate their period.

Typical orbital periods for those are <10 hr, so samples days or weeks apart would be very unlikely to end up during the short (<1 hr) ingress/egress periods. Some systems have been observed to have more complex flux density/eclipse variations (e.g., Polzin et al. 2020), but still generally not the large degree of continuum flux variability seen here.

Similarly, the precession of a pulsar will result in emission that comes and goes with a timescale of hours (e.g., Zhu & Xu 2006). The multiple detections with fading behavior over 50 hr in 2021 February and multiple nondetections over three months make eclipsing and precession unlikely interpretations. Hence, we conclude the observed emission is unlikely to be due to common pulsar-related origins.

Magnetars are neutron stars with extreme strong magnetic fields (up to $\sim10^{15}$ G; Duncan & Thompson 1992; Kaspi & Beloborodov 2017). There are 31 known magnetars and magnetar candidates to date[30] (Olausen & Kaspi 2014), but only five are detected in the radio as pulsars (Camilo et al. 2006, 2007; Levin et al. 2010; Eatough et al. 2013; Shannon & Johnston 2013; Rea et al. 2013; Karuppusamy et al. 2020; Lower et al. 2020). All the radio detections of magnetars happened during periods of X-ray outburst (Kaspi & Beloborodov 2017; Esposito et al. 2021), and faded eventually. Magnetars with confirmed radio pulsations show large pulse-to-pulse variability, including pulse morphology (Kaspi & Beloborodov 2017) and polarization (e.g., Dai et al. 2019). The persistent X-ray luminosity for these radio magnetars is typically $\sim10^{33}$ erg s^{-1} (Rea et al. 2012), and can reach as high as $\sim10^{36}$ erg s^{-1} during an outburst (e.g., Rea & Esposito 2011). Our upper limit based on the Chandra observation is comparable to the persistent luminosity of radio magnetars but

much lower than those during outbursts (Figure 12). All radio magnetars show very high degrees of polarization, but their flat radio spectra (Shannon & Johnston 2013), in contrast to what we see for ASKAP J173608.2−321635, makes a magnetar an unlikely interpretation (although see Pearlman et al. 2018). Similarly, the rotation period of magnetars is typically ~1–10 s (Kaspi & Beloborodov 2017), and that range is excluded based on our MeerKAT searches for most sources (DM $\lesssim$ 1000 pc cm^{-3}, corresponding to $\lesssim6$ kpc based on YMW16; Figure 11). As we discussed earlier, pulsations can be smeared out due to scattering, but the GC magnetar PSR J1745−2900 has scattering of only 1.3 s at 1 GHz, considerably lower than that expected from DM models (Spitler et al. 2014; Pearlman et al. 2018), so we may actually be sensitive to higher DMs than Figure 11 implies. Regardless, higher radio frequency observations may help to rule out or confirm a magnetar origin. We noted that our search did not exclude sources with extreme long period, such as an ultra long period magnetar 1E 161348-5055.1 (with a rotation period of 6.67 hr, De Luca et al. 2006). Further monitoring observations may help us find such periodic activity.

3.3. Other Transient Classes

We now consider whether ASKAP J173608.2−321635 could be an X-ray binary or extragalactic transient. The polarization and extremely steep spectrum are inconsistent with expectations for emission produced by a steady jet ($\alpha \sim 0$ at these radio frequencies) such as from low-mass X-ray binaries, or optically thin ejecta ($\alpha \sim -0.7$) such as gamma-ray bursts (e.g., Fender 2006). The short timescale ($\sim$days) of our source also rules out sources such as supernovae ($\sim$years; e.g., Dubner & Giacani 2015) and tidal disruption events ($\sim$months; e.g., Gezari 2021).
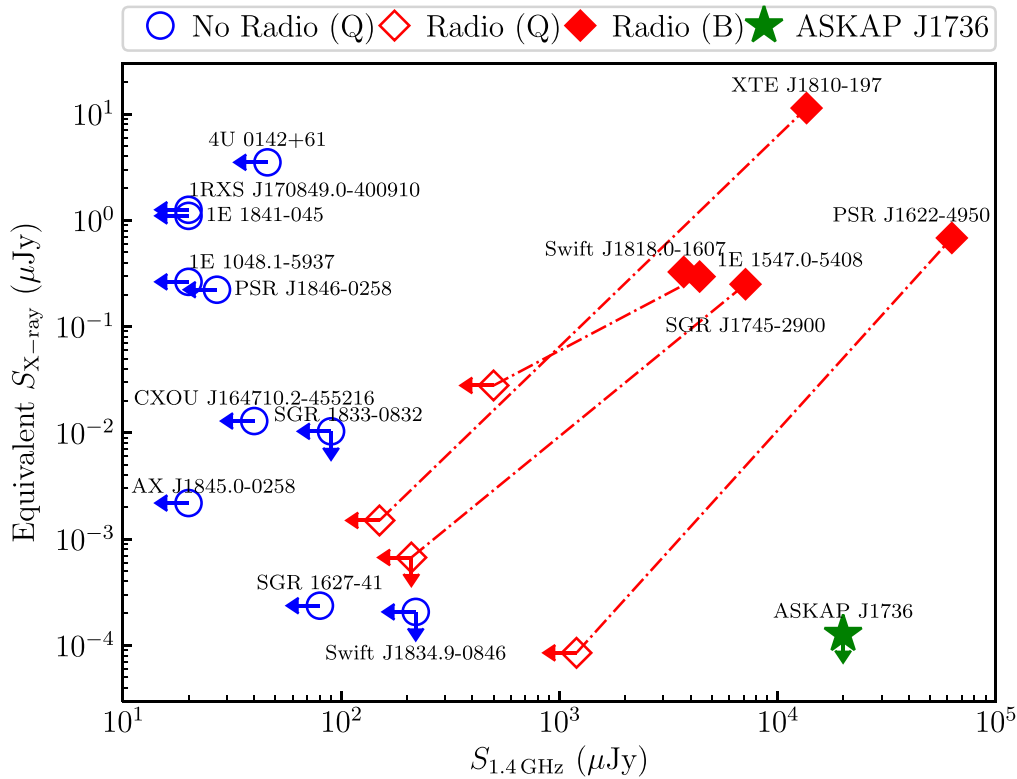

Figure 12. Equivalent X-ray spectral flux density vs. radio flux density for magnetars from the McGill Online Magnetar Catalog (Olausen & Kaspi 2014), along with ASKAP J173608.2−321635 (X-ray upper limit from the Chandra observation). We show magnetars with no radio pulsation as blue circles, magnetars with radio pulsations as red diamonds, and our source as a green star. Hollow markers and solid markers represent the source in the quiescent (Q) and outburst (B) state, respectively. The red lines connect the same source but with a different state. There are some missing or outdated values in the original catalog. We used new 1.4 GHz flux densities for Swift J1818.0−1607 (Lower et al. 2020), SGR J1745−2900 (Shannon & Johnston 2013, scaling the flux to 1.4 GHz with a spectral index of −1), and PSR J1622−4950 (Camilo et al. 2018). We adopt the unabsorbed X-ray flux for five magnetars at outburst state from Halpern et al. (2008), Camilo et al. (2018), Mori et al. (2013), Gotthelf et al. (2019), Esposito et al. (2020). Note that the radio flux density at an outburst state may not match the X-ray flux corresponding to the same outburst event, as not all sources were measured in both bands for the same outbursts. Radio fluxes of magnetars can be very variable on very short timescales and we used the average flux density here.

3.4. Variability Due to Extrinsic Effects

The large variability ($\sim$100×) is inconsistent with standard diffractive scintillation, which has a modulation index of order unity (e.g., Cordes & Lazio 1991; Narayan 1992) for compact sources. Refractive scintillation will produce even less variability, particularly due to the proximity of ASKAP J173608.2−321635 to the GC. While the total electron column density is unclear due to the unknown source distance, the expected variability due to refractive scintillation at 900 MHz ranges from a few tens of percent if it is nearby, to as little as 2% if it is more distance (Walker 1998; Cordes & Lazio 2002).

Intraday variables (IDVs) similarly have typical modulation of up to a factor of two (e.g., Quirrenbach et al. 1992), although it can be a slightly higher (e.g., Dennett-Thorpe & de Bruyn 2000). The linearly polarized flux can vary with higher amplitude and on faster timescales, but the polarization fraction is <10% (Kraus et al. 2003), so inconsistent with ASKAP J173608.2−321635.

However, we consider whether the observed emission could be caused by other forms of extrinsic variability, or a combination of both extrinsic and intrinsic effects. For example, one could invoke a compact radio source undergoing an extreme scattering event (ESE; e.g., Fiedler et al. 1987; Bannister et al. 2016), in which the emission is lensed by plasma in the intervening medium; however, this does not explain the high circular polarization we observe. In this case,

the lightcurve variability would be caused by propagation effects, while the change in polarization between the two periods of detectability would be intrinsic to the source.

Similar variability could be caused by gravitational lensing or plasma lensing. In general, gravitational lensing is achromatic while plasma lensing is highly chromatic (e.g., Wagner & Er 2020), but this is only true when the source is unresolved by the lens. If the source has finite size with spectral variations across it, then even gravitational lensing can have a chromatic effect as different regions are magnified/demagnified. For instance, a star with an active region could have different parts of that region magnified, which could increase the radio flux relative to other bands (Section 3.1) and give rise to highly polarized emission. However, it might still be difficult to explain multiple lensing events with similar magnifications. Further multiwavelength searches during bright states and better characterization of the lightcurve could help resolve this scenario.

3.5. A GCRT-like Interpretation

As the source is located only 4 degrees from the GC, we consider whether it could be another GCRT.

The GCRT sources share some properties with ASKAP J173608.2−321635. GCRT J1742−3001 has a spectral index of $\lesssim$−2 and GCRT J1745−3009 has a spectral index varying from −4 to −13, while that for our source varies from −2.7 to −5.6.

Both our source and GCRT J1745–3009 are highly polarized. GCRT J1745–3009 was ∼100% circularly polarized at 325 MHz (Roy et al. 2010). Our source was found to be 100% linearly polarized at ∼1.6 GHz and as high as ∼40% circularly polarized at ∼0.9 GHz. The source would have a flux density of ∼0.25 Jy extrapolated to 300 MHz, which is comparable to that for GCRT J1745–3009 (∼0.3 Jy). There is no X-ray detection for any of the GCRT sources when they are radio-bright.

However, some properties of our source are different from those of the GCRTs. GCRT J1745–3009 is thought to be a coherent emitter based on the very rapid variability (∼10 min), while our source shows no rapid variability and therefore may not emit coherently. The variability timescale for GCRT J1742–3001 is of order of one month, comparable with the initial "flare" detected in ASKAP but much longer than the timescale for the latest detections. GCRT J1745–3009 varies on much faster timescales: it emits flare-like emission for about 10 minutes out of a 77 minute period at a relative constant flux density. Hyman et al. (2007) showed that GCRT J1745–3009 has been detected in three different states. We have detected ASKAP J173608.2−321635 in two significant observation states so far (bright for a week versus fast fading). In general the sparse observations of ASKAP J173608.2−321635 and the GCRTs limits conclusions based on their temporal properties, and it is not even clear that all of the GCRTs share a common origin. Further monitoring will help resolve this.

4. Conclusions

We have presented the discovery and characterization of ASKAP J173608.2−321635: a highly polarized, variable radio source located near the GC and with no clear multiwavelength counterpart. We have largely ruled out most possible origins of ASKAP J173608.2−321635 including stars, normal neutron stars, and X-ray binaries. An intriguing remaining possibility comes from similarities to steep-spectrum radio sources discovered in recent imaging surveys (e.g., de Gasperin et al. 2018; Maan et al. 2018). Galactic sources with steep spectra are usually pulsars (e.g., Bates et al. 2013). However, pulsation searches for most of these sources have been unsuccessful (e.g., Crawford et al. 2000; Maan et al. 2018; Hyman et al. 2019; Crawford et al. 2021). As discussed by Maan et al. (2018) and de Gasperin et al. (2018), the explanations for unsuccessful pulsar searching include short period or eccentric binary systems (Ng et al. 2015), scattering in the interstellar medium, bias toward short period pulsars in the searching, or alignment of the magnetic and rotation axes (Perry & Lyne 1985). Our searches, especially the short MeerKAT observations, should have had sufficient sensitivity to detect binary systems, but the other two effects may be at play here as well. Or, these sources along with ASKAP J173608.2−321635 may belong to a new class of steep spectrum sources, possibly related to the GCRTs. In order to constrain the origin of ASKAP J173608.2−321635, continued radio monitoring, pulsations searches at higher frequencies, and multiwavelength observations are necessary.

ASKAP J173608.2−321635 is one of the first sources identified from our searches for transient, polarized sources in the VAST-P1 Survey (Murphy et al. 2021), and while it is among the most extreme in terms of its variability and polarization properties, it is not the only transient polarized source. However, most other such sources have straightforward identification with known stars (Murphy et al. 2021;

J. Pritchard et al. 2021, in preparation). Some do not, and these are the subject of further investigation (e.g., Y. Wang et al. 2021, in preparation). ASKAP J173608.2−321635 is further notable for its location toward the GC, although we do not yet know whether that is a coincidence or if that location is related to its nature: similar questions could be raised about the GCRT sources. Future comprehensive searches will quantify the exact number of such sources at different locations in the sky, including the Galactic plane, high-latitude regions, and the Magellanic Clouds (see Murphy et al. 2021 for the VAST Pilot-1 sky coverage). We found three variable sources above a modulation index of 0.9, from which ASKAP J173608.2−321635 easily stood out as it is the most variable source, the only polarized source, and the only source with no clear infrared counterpart. Given that ASKAP J173608.2−321635 is typically not detected and can turn off on timescales from several weeks to as quickly as a day, our sparse sampling (12 epochs over 16 months) suggests that there could be other similar sources in these fields. Increasing the survey cadence and comparing the results of this search to other regions will help us understand how truly unique ASKAP J173608.2−321635 is and whether it is related to the Galactic plane, which should ultimately help us deduce its nature.

(Hunter 2007), scipy (Virtanen et al. 2020), astropy (Astropy Collaboration et al. 2013, 2018).

Appendix
Polarization Verification

ASKAP J173608.2−321635 appears to be circularly polarized. We examined if the Stokes V detection is intrinsic or is the result of polarization leakage. We identified a few field sources with Stokes V detections at $>5\sigma$ significance in individual observations. As shown in Figure A1, the field sources with Stokes V detections are usually bright sources (detection S/N < 100), and Stokes V detections are due to a modest level of leakage (<1%). We can confirm that the circular polarization from our source is real, as the fractional circular polarization is much higher than 1% (also see Kaplan et al. 2019).

We attempted to verify whether the change in rotation measure for ASKAP J173608.2−321635 was due to instrumental effects or if it was intrinsic to ASKAP J173608.2−321635. Besides measuring the RM value based on RM-synthesis and after RMClean, we also used a direct $\lambda^2 - \chi$ fitting method to measure the RMs. As is shown in Figure A2 the RMs we measured from different methods are consistent and both methods show clear changes between the epochs. Stokes Q and Stokes U spectra (Figure A3) clearly show that the RM is different in the two epochs. We also found a linearly polarized field source (J173641.8−320029) with RM of $+259.9 \pm 1.9$ rad m^{-2} and $+256.2 \pm 2.2$ rad m^{-2} in the two epochs. This field source demonstrates that the RM stability between epochs is suitable to draw the conclusion about the temporal variability of ASKAP J173608.2−321635's RM.

The absence of a dedicated polarization calibration means that we cannot trust the absolute intrinsic polarization angle of our data. However, the changes of intrinsic polarization angle between epochs for ASKAP J173608.2−321635 and the field source
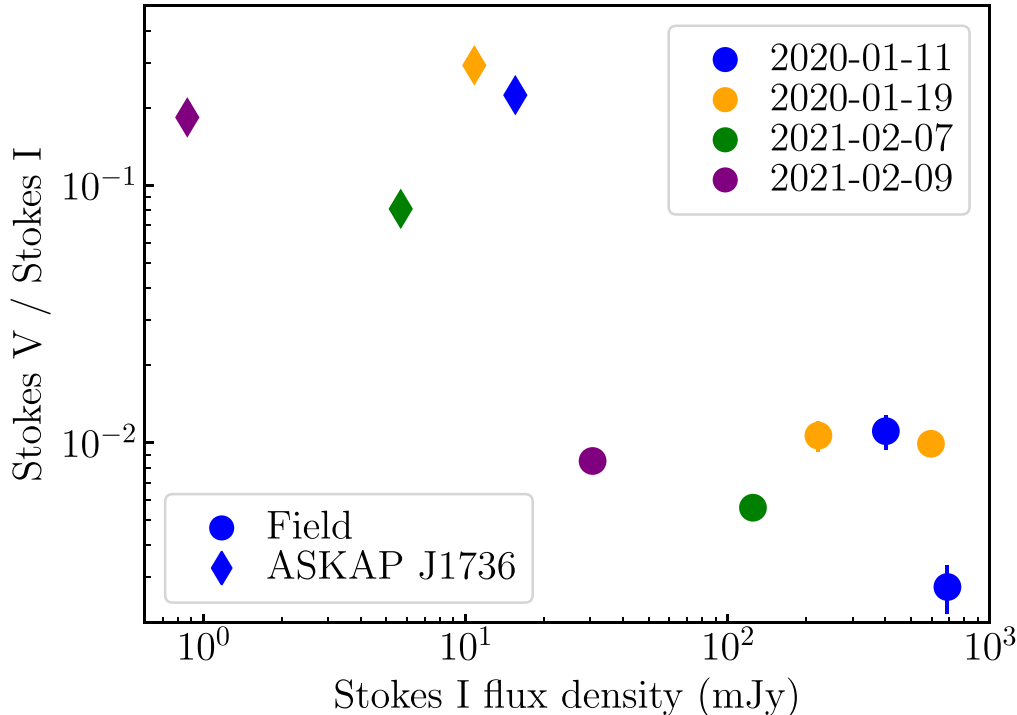

Figure A1. Fractional circular polarization in our images. We show the V/I flux density fraction against Stokes I flux density in four ASKAP observations with V/I detections. ASKAP J173608.2−321635 is shown as a diamond, and field sources (dominated by leakage) are shown as circles. All sources are detected at $>5\sigma$ in the Stokes V images, but the field sources have $V/I < 1\%$.
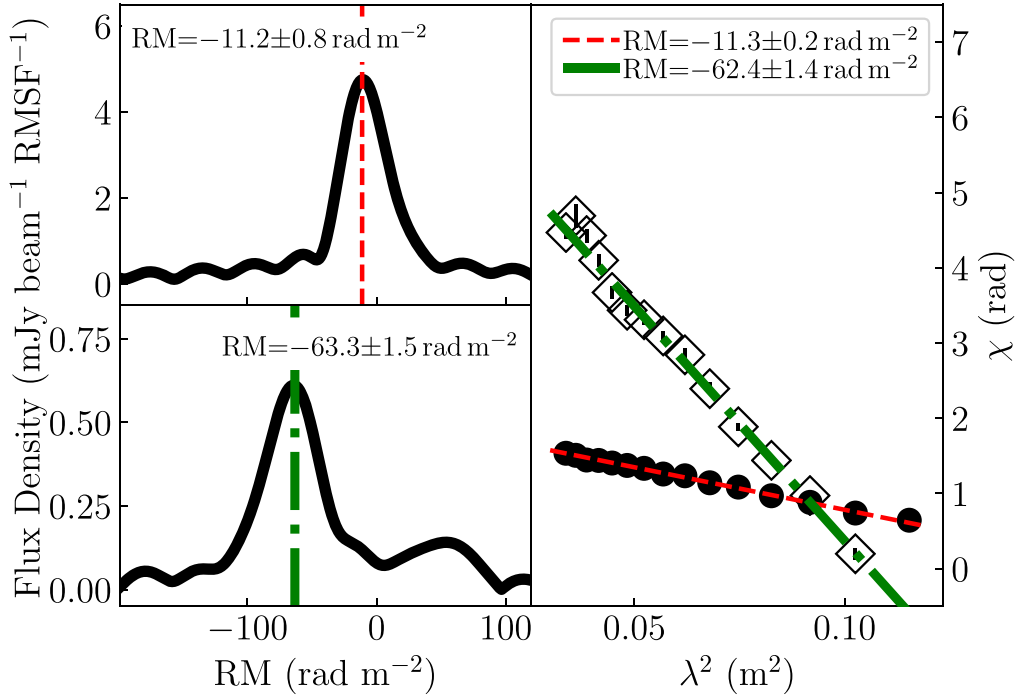
Figure A2. Faraday dispersion function (FDF) plot and $\lambda^2 - \chi$ (relative position angle) plot. The left side shows the FDF plots (with RMclean run), where the upper left panel is for 2021 February 7 (red dashed) and the lower left panel for 2021 February 9 (green dashdot). The right side shows the $\lambda^2 - \chi$ plot with best-fit lines to each observation, where circles and the red dashed line correspond to 2021 February 7 and diamonds and the green dashdot line correspond to 2021 February 9. We also show the RMs measured by different methods (in units of $\mathrm{rad\,m^{-2}}$) on each panel: Left—RM-synthesis; Right—direct $\lambda^2 - \chi$ fitting.
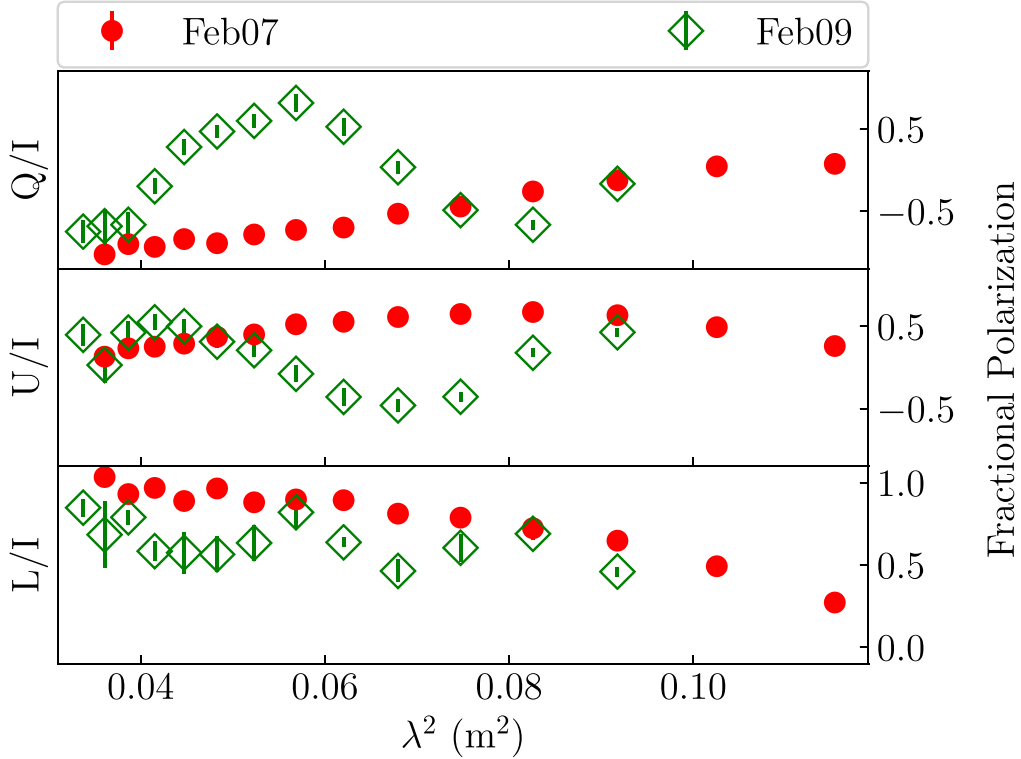

Figure A3. Fractional Stokes Q, U, and linear polarization as a function of λ^2. Red circles show the data from 2021 February 7, while green diamonds show the data from 2021 February 9.

(J173641.8−320029) are consistent. The intrinsic polarization angle for our source changed from 109.7 ± 0.7 deg to 18.6 ± 5.4 deg, while that for the field source changed from 116.0 ± 20.0 deg to 23.9 ± 22.6 deg. Therefore it is likely that the intrinsic polarization angle for ASKAP J173608.2−321635 did not change between epochs.

ORCID iDs

Ziteng Wang ⓘ https://orcid.org/0000-0002-2066-9823
David L. Kaplan ⓘ https://orcid.org/0000-0001-6295-2881
Tara Murphy ⓘ https://orcid.org/0000-0002-2686-438X
Emil Lenc ⓘ https://orcid.org/0000-0002-9994-1593
Shi Dai ⓘ https://orcid.org/0000-0002-9618-2499
Ewan Barr ⓘ https://orcid.org/0000-0001-8715-9628
Dougal Dobie ⓘ https://orcid.org/0000-0003-0699-7019
B. M. Gaensler ⓘ https://orcid.org/0000-0002-3382-9558
George Heald ⓘ https://orcid.org/0000-0002-2155-6054
James K. Leung ⓘ https://orcid.org/0000-0002-9415-3766
Andrew O'Brien ⓘ https://orcid.org/0000-0003-4609-2791
Sergio Pintaldi ⓘ https://orcid.org/0000-0003-3860-5825
Joshua Pritchard ⓘ https://orcid.org/0000-0003-1575-5249
Nanda Rea ⓘ https://orcid.org/0000-0003-2177-6388
Gregory R. Sivakoff ⓘ https://orcid.org/0000-0001-6682-916X
B. W. Stappers ⓘ https://orcid.org/0000-0001-9242-7041
Adam Stewart ⓘ https://orcid.org/0000-0001-8026-5903
E. Tremou ⓘ https://orcid.org/0000-0002-4039-6703
Yuanming Wang ⓘ https://orcid.org/0000-0003-0203-1196
Patrick A. Woudt ⓘ https://orcid.org/0000-0002-6896-1655
Andrew Zic ⓘ https://orcid.org/0000-0002-9583-2947

References

Anderson, C. S., O'Sullivan, S. P., Heald, G. H., et al. 2019, MNRAS, 485, 3600
Astropy Collaboration, Price-Whelan, A. M., Sipőcz, B. M., et al. 2018, AJ, 156, 123
Astropy Collaboration, Robitaille, T. P., Tollerud, E., et al. 2013, A&A, 558, A33
Bannister, K. W., Stevens, J., Tuntsov, A. V., et al. 2016, Sci, 351, 354
Barr, E. D. 2017, in IAU Symp. 337, Pulsar Astrophysics the Next Fifty Years (Cambridge: Cambridge Univ. Press), 175
Barrett, P., Dieck, C., Beasley, A. J., Mason, P. A., & Singh, K. P. 2020, AdSpR, 66, 1226
Bates, S. D., Lorimer, D. R., & Verbiest, J. P. W. 2013, MNRAS, 431, 1352
Benz, A. O., & Güdel, M. 1994, A&A, 285, 621
Berger, E., Basri, G., Fleming, T. A., et al. 2010, ApJ, 709, 332
Bertin, E., & Arnouts, S. 1996, A&AS, 117, 393
Bhat, N. D. R., Cordes, J. M., Camilo, F., Nice, D. J., & Lorimer, D. R. 2004, ApJ, 605, 759
Bower, G. C., Roberts, D. A., Yusef-Zadeh, F., et al. 2005, ApJ, 633, 218
Broderick, J. W., Fender, R. P., Breton, R. P., et al. 2016, MNRAS, 459, 2681
Burningham, B., Hardcastle, M., Nichols, J. D., et al. 2016, MNRAS, 463, 2202
Burrows, D. N., Hill, J. E., Nousek, J. A., et al. 2005, SSRv, 120, 165
Camilo, F., Ransom, S. M., Halpern, J. P., et al. 2006, Natur, 442, 892
Camilo, F., Ransom, S. M., Halpern, J. P., & Reynolds, J. 2007, ApJL, 666, L93
Camilo, F., Ransom, S. M., Halpern, J. P., & Roshi, D. A. 2021, ApJ, 917, 67
Camilo, F., Scholz, P., Serylak, M., et al. 2018, ApJ, 856, 180
Chen, W., Barr, E., Karuppusamy, R., Kramer, M., & Stappers, B. 2021, JAI, submitted
Chiti, A., Chatterjee, S., Wharton, R., et al. 2016, ApJ, 833, 11
Condon, J. J., Cotton, W. D., Greisen, E. W., et al. 1998, AJ, 115, 1693
Cordes, J. M., & Lazio, T. J. 1991, ApJ, 376, 123
Cordes, J. M., & Lazio, T. J. W. 2002, arXiv:astro-ph/0207156
Crawford, F., Kaspi, V. M., & Bell, J. F. 2000, AJ, 119, 2376
Crawford, F., Margeson, J., Nguyen, B., et al. 2021, RNAAS, 5, 21
Dai, S., Lower, M. E., Bailes, M., et al. 2019, ApJL, 874, L14
Davies, R. D., Walsh, D., Browne, I. W. A., Edwards, M. R., & Noble, R. G. 1976, Natur, 261, 476
de Gasperin, F., Intema, H. T., & Frail, D. A. 2018, MNRAS, 474, 5008
De Luca, A., Caraveo, P. A., Mereghetti, S., Tiengo, A., & Bignami, G. F. 2006, Sci, 313, 814
Demorest, P. B., Ferdman, R. D., Gonzalez, M. E., et al. 2013, ApJ, 762, 94
Dennett-Thorpe, J., & de Bruyn, A. G. 2000, ApJL, 529, L65

Desvignes, G., Eatough, R. P., Pen, U. L., et al. 2018, ApJL, 852, L12
Donner, J. Y., Verbiest, J. P. W., Tiburzi, C., et al. 2020, A&A, 644, A153
Driessen, L. N., McDonald, I., Buckley, D. A. H., et al. 2020, MNRAS, 491, 560
Dubner, G., & Giacani, E. 2015, A&ARv, 23, 3
Dulk, G. A. 1985, ARA&A, 23, 169
Duncan, R. C., & Thompson, C. 1992, ApJL, 392, L9
Eatough, R. P., Falcke, H., Karuppusamy, R., et al. 2013, Natur, 501, 391
Esposito, P., Rea, N., Borghese, A., et al. 2020, ApJL, 896, L30
Esposito, P., Rea, N., & Israel, G. L. 2021, in Timing Neutron Stars: Pulsations, Oscillations and Explosions, ed. T. M. Belloni, M. Méndez, & C. Zhang (Berlin: Springer), 97
Farnes, J. S., Gaensler, B. M., & Carretti, E. 2014, ApJS, 212, 15
Fender, R. 2003, Ap&SS, 288, 79
Fender, R. 2006, Compact Stellar X-Ray Sources (Cambridge: Cambridge Univ. Press), 381
Fender, R., Stewart, A., Macquart, J. P., et al. 2015, in Proc. of Science 215, Advancing Astrophysics with the Square Kilometre Array (AASKA14) (Trieste: SISSA), 51
Ferrière, K. M. 2001, RvMP, 73, 1031
Fiedler, R. L., Dennison, B., Johnston, K. J., & Hewish, A. 1987, Natur, 326, 675
Fruchter, A. S., Stinebring, D. R., & Taylor, J. H. 1988, Natur, 333, 237
Gehrels, N., Chincarini, G., Giommi, P., et al. 2004, ApJ, 611, 1005
Gezari, S. 2021, ARA&A, in press, arXiv:2104.14580
Gotthelf, E. V., Halpern, J. P., Alford, J. A. J., et al. 2019, ApJL, 874, L25
Güdel, M., & Benz, A. O. 1993, ApJL, 405, L63
Guzman, J., Whiting, M., Voronkov, M., et al. 2019, ASKAPsoft: ASKAP science data processor software, Astrophysics Source Code Library, ascl:1912.003
Hallinan, G., Bourke, S., Lane, C., et al. 2007, ApJL, 663, L25
Halpern, J. P., Gotthelf, E. V., Reynolds, J., Ransom, S. M., & Camilo, F. 2008, ApJ, 676, 1178
Hammersley, P. L., Garzón, F., Mahoney, T. J., López-Corredoira, M., & Torres, M. A. P. 2000, MNRAS, 317, L45
Han, J. L. 2017, ARA&A, 55, 111
Helfand, D. J., Schnee, S., Becker, R. H., White, R. L., & McMahon, R. G. 1999, AJ, 117, 1568
Heywood, I. 2020, oxkat: Semi-automated imaging of MeerKAT observations, Astrophysics Source Code Library, ascl:2009.003
HI4PI Collaboration, Ben Bekhti, N., Flöer, L., et al. 2016, A&A, 594, A116
Hilmarsson, G. H., Michilli, D., Spitler, L. G., et al. 2021, ApJL, 908, L10
Hobbs, G., Manchester, R. N., Dunning, A., et al. 2020, PASA, 37, e012
Hotan, A. W., Bunton, J. D., Chippendale, A. P., et al. 2021, PASA, 38, e009
Hunter, J. D. 2007, CSE, 9, 90
Hurley-Walker, N., Callingham, J. R., Hancock, P. J., et al. 2017, MNRAS, 464, 1146
Hutschenreuter, S., Anderson, C. S., Betti, S., et al. 2021, A&A, submitted, arXiv:2102.01709
Hyman, S. D., Frail, D. A., Deneva, J. S., et al. 2019, ApJ, 876, 20
Hyman, S. D., Frail, D. A., Deneva, J. S., et al. 2021, MNRAS, 507, 3888
Hyman, S. D., Lazio, T. J. W., Kassim, N. E., & Bartleson, A. L. 2002, AJ, 123, 1497
Hyman, S. D., Lazio, T. J. W., Kassim, N. E., et al. 2005, Natur, 434, 50
Hyman, S. D., Roy, S., Pal, S., et al. 2007, ApJL, 660, L121
Hyman, S. D., Wijnands, R., Lazio, T. J. W., et al. 2009, ApJ, 696, 280
Intema, H. T., Jagannathan, P., Mooley, K. P., & Frail, D. A. 2017, A&A, 598, A78
Johnston, H. M., & Kulkarni, S. R. 1991, ApJ, 368, 504
Johnston, S., & Kerr, M. 2018, MNRAS, 474, 4629
Jonas, J. 2016, in Proc. of Science 277, MeerKAT Science: On the Pathway to the SKA (Trieste: SISSA), 1
Kao, M. M., Hallinan, G., Pineda, J. S., et al. 2016, ApJ, 818, 24
Kaplan, D. L., Dai, S., Lenc, E., et al. 2019, ApJ, 884, 96
Kaplan, D. L., Hyman, S. D., Roy, S., et al. 2008, ApJ, 687, 262
Karuppusamy, R., Desvignes, G., Kramer, M., et al. 2020, ATel, 13553, 1
Kaspi, V. M., & Beloborodov, A. M. 2017, ARA&A, 55, 261
Kellermann, K. I., & Pauliny-Toth, I. I. K. 1981, ARA&A, 19, 373
Kramer, M., Lyne, A. G., O'Brien, J. T., Jordan, C. A., & Lorimer, D. R. 2006, Sci, 312, 549
Kraus, A., Krichbaum, T. P., Wegner, R., et al. 2003, A&A, 401, 161
Labrie, K., Anderson, K., Cárdenes, R., Simpson, C., & Turner, J. E. H. 2019, in ASP Conf. Series, 523, Astronomical Data Analysis Software and Systems XXVI, ed. P. J. Teuben et al. (San Francisco, CA: ASP), 321
Lacy, M., Baum, S. A., Chandler, C. J., et al. 2020, PASP, 132, 035001
Lam, M. T., Ellis, J. A., Grillo, G., et al. 2018, ApJ, 861, 132

Lazio, J., Deneva, J. S., Bower, G. C., et al. 2006, JPhCS, 54, 110
Levin, L., Bailes, M., Bates, S., et al. 2010, ApJL, 721, L33
Lico, R., Gómez, J. L., Asada, K., & Fuentes, A. 2017, MNRAS, 469, 1612
Lorimer, D. R., & Kramer, M. 2012, Handbook of Pulsar Astronomy (Cambridge: Cambridge Univ. Press)
Lower, M. E., Shannon, R. M., Johnston, S., & Bailes, M. 2020, ApJL, 896, L37
Lynch, C. R., Lenc, E., Kaplan, D. L., Murphy, T., & Anderson, G. E. 2017, ApJL, 836, L30
Lyne, A. G. 2009, in Neutron Stars and Pulsars, ed. W. Becker (Berlin: Springer), 67
Maan, Y., Bassa, C., van Leeuwen, J., Krishnakumar, M. A., & Joshi, B. C. 2018, ApJ, 864, 16
Macquart, J.-P. 2003, NewAR, 47, 609
Macquart, J.-P., Wu, K., Hannikainen, D. C., Sault, R. J., & Jauncey, D. L. 2003, Ap&SS, 288, 105
Manchester, R. N., Hobbs, G. B., Teoh, A., & Hobbs, M. 2005, AJ, 129, 1993
McConnell, D., Hale, C. L., Lenc, E., et al. 2020, PASA, 37, e048
McMullin, J. P., Waters, B., Schiebel, D., Young, W., & Golap, K. 2007, in ASP Conf. Ser., 376, Astronomical Data Analysis Software and Systems XVI, ed. R. A. Shaw, F. Hill, & D. J. Bell (San Francisco, CA: ASP), 127
Minniti, D., Lucas, P. W., Emerson, J. P., et al. 2010, NewA, 15, 433
Mori, K., Gotthelf, E. V., Zhang, S., et al. 2013, ApJL, 770, L23
Murphy, T., Chatterjee, S., Kaplan, D. L., et al. 2013, PASA, 30, e006
Murphy, T., Kaplan, D. L., Stewart, A. J., et al. 2021, arXiv:2108.06039
Murphy, T., Mauch, T., Green, A., et al. 2007, MNRAS, 382, 382
Mutel, R. L., Morris, D. H., Doiron, D. J., & Lestrade, J. F. 1987, AJ, 93, 1220
Narayan, R. 1992, RSPTA, 341, 151
Ng, C., Champion, D. J., Bailes, M., et al. 2015, MNRAS, 450, 2922
Offringa, A. R., McKinley, B., Hurley-Walker, N., et al. 2014, MNRAS, 444, 606
Olausen, S. A., & Kaspi, V. M. 2014, ApJS, 212, 6
Osterbrock, D. E. 1989, Astrophysics of Gaseous Nebulae and Active Galactic Nuclei (Sausalito, CA: Univ. Science Books)
Pearlman, A. B., Majid, W. A., Prince, T. A., Kocz, J., & Horiuchi, S. 2018, ApJ, 866, 160
Pecaut, M. J., & Mamajek, E. E. 2013, ApJS, 208, 9
Perry, T. E., & Lyne, A. G. 1985, MNRAS, 212, 489
Pintaldi, S., Stewart, A., O'Brien, A., Kaplan, D., & Murphy, T. 2021, arXiv:2101.05898
Polzin, E. J., Breton, R. P., Bhattacharyya, B., et al. 2020, MNRAS, 494, 2948
Pritchard, J., Murphy, T., Zic, A., et al. 2021, MNRAS, 502, 5438
Quirrenbach, A., Witzel, A., Kirchbaum, T. P., et al. 1992, A&A, 258, 279
Ransom, S. M. 2001, PhD thesis, Harvard University

Rea, N., & Esposito, P. 2011, High-Energy Emission from Pulsars and their Systems (Berlin: Springer), 247
Rea, N., Esposito, P., Pons, J. A., et al. 2013, ApJL, 775, L34
Rea, N., Pons, J. A., Torres, D. F., & Turolla, R. 2012, ApJL, 748, L12
Readhead, A. C. S. 1994, ApJ, 426, 51
Reid, H. A. S., & Ratcliffe, H. 2014, RAA, 14, 773
Reid, I. N., Cruz, K. L., Kirkpatrick, J. D., et al. 2008, AJ, 136, 1290
Roberts, M. S. E. 2013, in IAU Symp. 291, Neutron Stars and Pulsars: Challenges and Opportunities after 80 Years, ed. J. van Leeuwen (Cambridge: Cambridge Univ. Press), 127
Roy, S., Hyman, S. D., Pal, S., et al. 2010, ApJL, 712, L5
Sault, R. J., Teuben, P. J., & Wright, M. C. H. 1995, in ASP Conf. Ser., 77, Astronomical Data Analysis Software and Systems IV, ed. R. A. Shaw, H. E. Payne, & J. J. E. Hayes (San Francisco, CA: ASP), 433
Shannon, R. M., & Johnston, S. 2013, MNRAS, 435, L29
Skrutskie, M. F., Cutri, R. M., Stiening, R., et al. 2006, AJ, 131, 1163
Sotomayor-Beltran, C., Sobey, C., Hessels, J. W. T., et al. 2013, A&A, 552, A58
Spitler, L. G., Lee, K. J., Eatough, R. P., et al. 2014, ApJL, 780, L3
Staelin, D. H. 1969, IEEEP, 57, 724
Staelin, D. H., & Reifenstein, E. C. I. 1968, Sci, 162, 1481
Stappers, B. W., Bailes, M., Lyne, A. G., et al. 1996, ApJL, 465, L119
Swinbank, J. D., Staley, T. D., Molenaar, G. J., et al. 2015, A&C, 11, 25
Vedantham, H. K., Callingham, J. R., Shimwell, T. W., et al. 2020, ApJL, 903, L33
Virtanen, P., Gommers, R., Oliphant, T. E., et al. 2020, NatMe, 17, 261
Wagner, J., & Er, X. 2020, A&A, submitted, arXiv:2006.16263
Wahl, H. M., McLaughlin, M., Gentile, P. A., et al. 2021, ApJ, submitted, arXiv:2104.05723
Wainscoat, R. J., Cohen, M., Volk, K., Walker, H. J., & Schwartz, D. E. 1992, ApJS, 83, 111
Walker, M. A. 1998, MNRAS, 294, 307
Wayth, R. B., Lenc, E., Bell, M. E., et al. 2015, PASA, 32, e025
Whittet, D. C. B. 1992, Dust in the Galactic Environment (Bristol: A. Hilger)
Williams, P. K. G., Cook, B. A., & Berger, E. 2014, ApJ, 785, 9
Yan, W. M., Manchester, R. N., Hobbs, G., et al. 2011, Ap&SS, 335, 485
Yao, J. M., Manchester, R. N., & Wang, N. 2017, ApJ, 835, 29
You, X. P., Hobbs, G., Coles, W. A., et al. 2007, MNRAS, 378, 493
Yuan, H. B., Liu, X. W., & Xiang, M. S. 2013, MNRAS, 430, 2188
Zavala, R. T., & Taylor, G. B. 2003, ApJ, 589, 126
Zhao, J.-H., Morris, M. R., & Goss, W. M. 2020, ApJ, 905, 173
Zhao, J.-H., Roberts, D. A., Goss, W. M., et al. 1992, Sci, 255, 1538
Zhu, W. W., & Xu, R. X. 2006, MNRAS, 365, L16
Zic, A., Stewart, A., Lenc, E., et al. 2019, MNRAS, 488, 559
Zyuzin, D., Zharikov, S., Shibanov, Y., et al. 2016, MNRAS, 455, 1746